An intrinsic oscillator underlies visual navigation in ants

Leo Clement, Sebastian Schwarz, Antoine Wystrach

An intrinsic oscillator underlies visual navigation in ants

Leo Clement*, Sebastian Schwarz and Antoine Wystrach

Centre de Recherches sur la Cognition Animale, CNRS, Université Paul Sabatier, Toulouse 31062 cedex 09, France

*Address of correspondence:
Léo Clément
Université Paul Sabatier
Centre de Recherches sur la Cognition Animale, CNRS
31062 Toulouse
Email: clement.leo@univ-tlse3.fr
Phone: +33561558444

Highlights

- Ants show regular oscillations while navigating.
- Amplitude of oscillations are modulated by both learnt and innate visual cues.
- This modulation optimizes the balance between exploration and exploitation.
- Oscillations are produced internally as reproduce with a simple neural model.

Abstract

Many insects display lateral oscillations while moving, but how they are produced and participate in visual navigation remains unclear. Here we show that visually navigating ants continuously display regular lateral oscillations coupled with variations of forward speed that strongly optimise the distance covered while simultaneously enabling them to scan left and right directions. This pattern of movement is produced endogenously and conserved across navigational contexts in two phylogenetically distant ant species. Moreover, the oscillations' amplitude can be modulated by both innate or learnt visual cues to adjust the exploration/exploitation balance to the current need. This lower-level motor pattern thus drastically reduces the degree of freedom needed for higher level strategies to control behaviour. The observed dynamical signature readily emerges from a simple neural-circuit model of the insect's conserved pre-motor area known as the lateral accessory lobe, offering a surprisingly simple but effective neural control, and endorsing oscillations as a core, ancestral way of moving in insects**.**

Keywords: insect navigation, time series analysis, intrinsic oscillator, lateral accessory lobe.

Introduction

Navigating through space implies both to acquire information (exploration) and to use this information to move in the correct direction (exploitation). A way to acquire information is to sample the environment by actively moving. Such 'active-sampling' is common across the animal kingdom spanning from invertebrates [1–3] to vertebrates [4–8]. However, active sampling entails movements that are typically different than moving towards the goal and thus requires the animal to solve a trade-off. Achieving a balance between sampling actions (exploration) and goal-directed actions (exploitation) lies at the core of the behavioural control, but how it is achieved and evolved in animals remains unclear.

A way of sampling the world is through the production of regular alternations between left and right turns along the path: lateral oscillations. Lateral oscillations are observed in wide range of taxa (vertebrates [8,9]; invertebrates[10–14]) and have been mainly studied in the context of olfactory behaviours such as plume following in moths[12,15–17], trail following in ants[18] or odour gradient climbing in Drosophila larvae[14] and *Caenorhabditis elegans*[19]. The intrinsic production of oscillations enables an efficient sampling of odour across locations and models show that oscillations modulated by odour perception enables to reach the source in a remarkably effective way[14,19,20].

Modelling studies have shown that lateral oscillations can also be useful for visual navigation. For instance, having the amplitude of oscillation modulated by the familiarity of the perceived visual scenes, can produce robust visual navigational behaviours such as route-following[21] or homing[22], and captures particular behavioural signatures observed in ants[23]. Moreover, visually guided insects such as ants[23–28], wasps[29,30] or bumblebees[31] do display oscillations, whose expression appears to be coupled with visual perceptual cues. But whether these lateral oscillations are produced internally, how exactly they interact with visual cues and how they participate to the visual navigational task remains unclear.

We focused on the expression of oscillations in two ecologically and phylogenetically distant ant species: *Myrmecia croslandi* are solitary foragers relying heavily on vision[23,27,32–34] ; and *Iridomyrmex purpureus* that uses mass recruitment and pheromone trials but also other modalities for navigation[35]. The replication of the experiments in two distant species enables to tell apart whether the observed signatures are species-specific or shared across ants.

As most central place foragers, these ants species are known to rely on two main strategies to guide their foraging journeys [33,35]. The first strategy, commonly called Path Integration, allows individuals to continuously estimate the distance and compass direction that separates them from their nest (or other starting points) during their foraging trip[36–38]. The second, commonly called view-based navigation, involves the learning and subsequent recognition of the learnt visual panorama[38–40]. To see how these navigational strategies interact with oscillations, we mounted ants on a spherical treadmill device[41] (see Star methods), directly in their natural environment. This device enables to record the ants motor behaviour in detail, without interference of the uneven ground, while facilitating the control of the surrounding visual cue perceived. We characterised whether the obtained trajectories show a regular oscillatory pattern of movements and how these patterns are influenced by the presence or absence of: (1) visual input, (2) learnt visual terrestrial cues, (3) path integration homing vector and (4) rotational visual feedback. In both species, our results revealed the presence of a conserved pattern of oscillations generated intrinsically, which comprises both angular and forward velocity components. This pattern of movement provides a remarkable trade-off between exploration and exploitation and the amplitude of the oscillations can be flexibly adjusted by visual information in a way that is adapted to the navigational tasks at hand. Finally, we propose a simple neural circuit model of reciprocal inhibition between left and right pre-motor area to explore how these movement dynamics could be produced.

Results

Ants mounted on the trackball display their natural navigational behaviour

We first investigated whether ants mounted on the trackball display their natural navigational behaviours across different experimental conditions. When released on the ground in their natural environment, both species studied here (*Myrmecia croslandi* and *Iridomyrmex purpureus* see Figure S1) are known to rely on learnt terrestrial cues as well as, to a lesser extent, on Path Integration (PI)[23,33–35]. We first tethered ants and placed them on top of the trackball in a way that enabled them to physically rotate and control their actual body orientation[41] (Figure S2). The trackball was placed in three distinct visual conditions: (1) along the individual ant's familiar route (F) therefore in presence of familiar terrestrial cues; (2) in an unfamiliar location (U) 50 meters away from their usual route; or (3) without any visual input: in complete darkness (D). For each of these visual conditions, ants were tested either with (full-vector (FV) ants) or without (zero-vector (ZV) ants) PI information. While FV ants were captured at their feeding place and thus possess a PI homing vector pointing in the food-to-nest compass direction, ZV ants were caught just before entering their nest and thus no longer possess a PI homing vector.

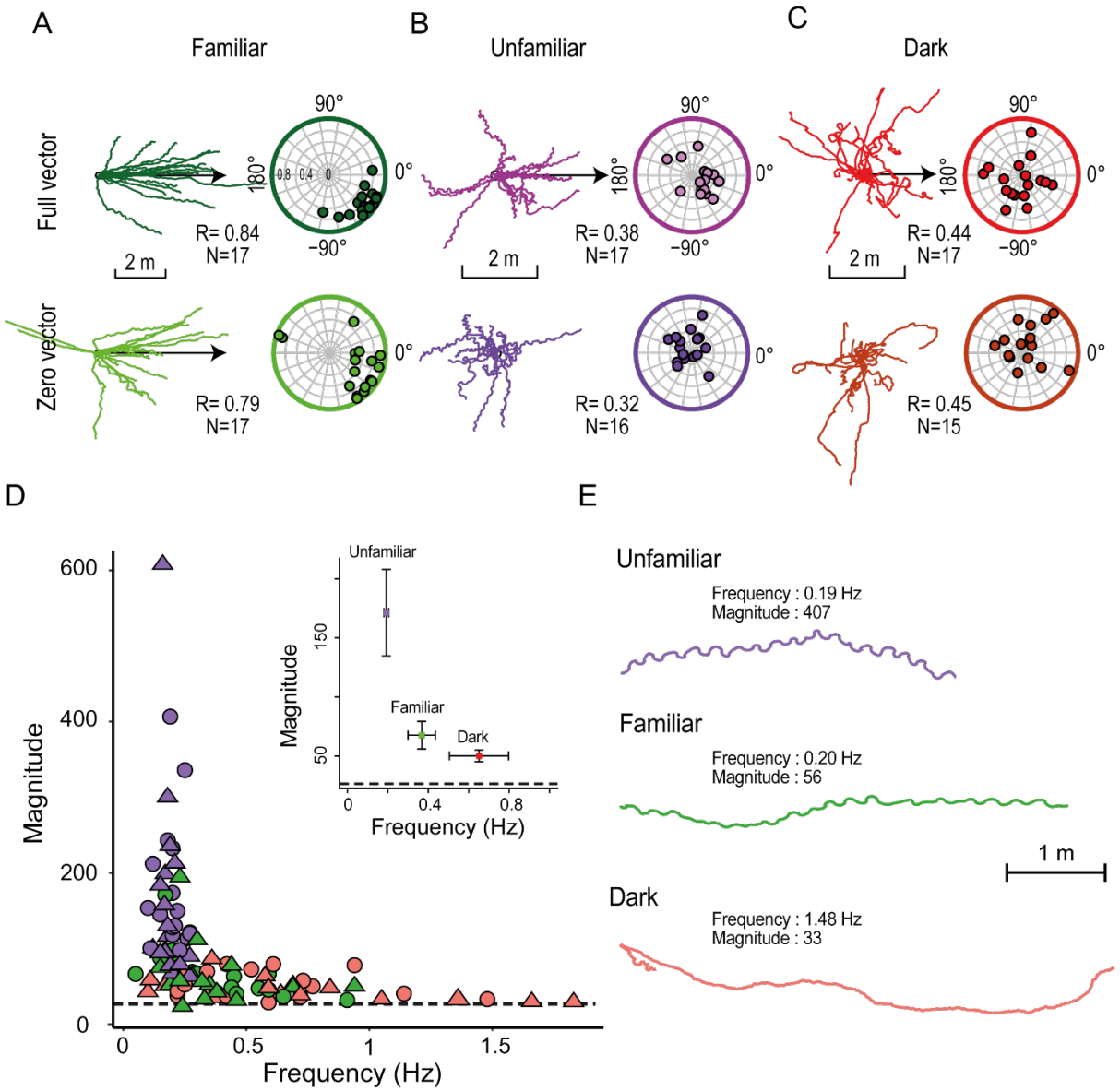

Figure 1. Oscillation characteristics vary across visual conditions. Trajectories of *M. croslandi* tested on the trackball in a familiar panorama along their known route ((A) green), an unfamiliar panorama ((B) purple) or in the dark ((C) red). For each condition, individuals were tested either with (full-vector, top row) or without (zero-vector, bottom row) path integration information. Reconstructed paths over 60 s are displayed relative to the real (in familiar) or theoretical (in full-vector) direction of the nest (arrow). In the circular plots, each dot indicates the average circular vector calculated over the entire path of an individual, showing the mean direction and the average vector length (i.e., a point closer to the periphery indicates straighter paths). The R values ('Straightness' between 0 and 1) indicate the length of the average resulting vector of the population. The direction (in familiar terrain) or theoretical direction (for FV in unfamiliar terrain) of the nest is 0°. (D) The graphs show the frequency and spectral density magnitude of the dominant oscillation (highest magnitude) for method see method see Figure S2). High frequencies indicate a fast-oscillatory rhythm and high magnitudes indicate a strong presence of this oscillation. Individuals were tested within a familiar panorama (green), an unfamiliar panorama (purple) or in the dark (red). Symbols indicate whether the state of the Path Integration vector was full (round) or zero (triangles) at the beginning of the experiment. Inserts show the mean frequency against the mean magnitude of each visual condition with the associated 95% confidence interval around the

mean. The dashed black line represents the mean of the spectral density peak magnitudes resulting from 200 Gaussian white noise signals. (E) example path for each condition for *M. croslandi* across 100s.

Irrespectively of the PI state (FV or ZV), ants mounted on the trackball within their familiar visual route (i.e., in the presence of learnt terrestrial cues) displayed paths that were oriented toward the nest direction (Figure 1A; Rayleigh test with nest as theoretical direction ps: FV & ZV < 0.001), proving that they recognised and used the familiar terrestrial cues to orient even without PI information (ZV). When tested in unfamiliar surroundings, FV ants were oriented towards the theoretical direction of the nest as indicated by their PI (Figure 1B first row; Rayleigh test with PI as theoretical direction p: FV< 0.001); but ZV ants (Figure 1B second row) showed random orientations (Rayleigh test p: ZV=0.443). This confirms that the distant release points were indeed unfamiliar to the ants and that the ants relied on their PI when tested as FV ants. When tested in total darkness, ants displayed randomly orientated paths in all conditions (Figure 1C; Rayleigh test p: FV=0.354; ZV=0.360;), showing that the chosen dark condition was effective in preventing the ants to use neither terrestrial nor celestial cues for orientation. Overall, these results demonstrate that *M. croslandi* foragers rely on learnt terrestrial cues as well as their PI to navigate when mounted on the trackball system (Figure 1).

We then looked at the individual's path straightness (R values in Figure 1 that indicate whether the ant's travel directions were rather constant across time (R=1) or not (R=0)). Independent of the PI state, the ants' paths were straighter in familiar terrain as compared to the other conditions (Figure 1; Familiar vs. Unfamiliar & Familiar vs. Dark: p*s* < 0.001), showing that the recognition of learnt terrestrial cues was most effective at helping the ant to maintain a constant direction of travel. With regards to the effect of PI state, there was no difference on the path straightness within each visual condition (FV vs ZV ps <0.1, Figure 1)

Overall, these results show that *M.croslandi* rely greatly on learnt visual cues and to a lesser extent on their PI. The latter still enables them to guide their general direction in unfamiliar terrain, but has only a limited impact on their path's straightness. Qualitatively similar results were obtained with our second species *I. purpureus* (see Figure S1). These results are consistent with what is observed in these species when navigating on their natural grounds [33,35].

Ants display regular lateral oscillations

To determine whether ants display regular lateral oscillations – that is, alternate between left and right turns at a steady rhythm – we first used our video recordings to track the ant's change in body orientation when mounted on the trackball. The body angular velocity signal is independent of the ant's actual forward movement and thus a direct reading of its motor control for turning. We conducted a Fourier analysis on autocorrelation coefficients of the angular velocity time series to obtain a 'power spectral density' (PSD) (see Figure S2 C-E) for detailed method). This PSD provides information about the regularity and frequency of oscillation, with higher magnitude values (y axis; Figure S2E) indicating more regular oscillation at the corresponding frequency (x axis; Figure S2E). For each ant, we selected the frequency corresponding to the highest magnitude (peak), that is, the most salient rhythm in the signal. In all experimental conditions, the obtained peak fell in the expected range of 0.2 to 1.5 Hz, as observed in other insect species[14,42]. It should be noted that this rhythm is 10 to 50 times slower than ants' typical stepping frequency[43] and thus are not the consequence of their rhythmic walking gait and hence must be the product of a different oscillatory mechanism. For both species, the obtained highest PSD magnitudes obtained with the ants signal were higher than the ones obtained with a Gaussian white noise (Figure 1D dashed line; Wilcoxon one-tail test: $p \leq 0.001$, see Figure S3 A, C for *I. purpureus*), showing that ants

displayed lateral oscillations with a higher regularity than random. We also replicated the same analysis using tracks of *M. croslandi* ants recorded directly on the ground while displaying learning walks around their nest (Figure S4), which confirms that these regular oscillations are not a consequence of being mounted on the trackball set-up.

The navigational context modifies the regularity and frequency of oscillations

We tested whether the visual condition and the state of the path integrator influenced how regular the oscillations are, which can be measure with the magnitude of the individuals' power spectral density peak, (PSD, see S2 C-E for individual example and method) (Figure 1D, E). The statistical model revealed no interaction between both effects (AIC=-198.8, $F_{2,101}$=0.434, p=0.647) however the additive model (i.e., without interaction AIC=-215.8) explains the variation of the magnitude peaks relatively well (R^2 marginal=56% & conditional=67%). PI state did not affect the regularity of oscillations (PSD peak magnitudes (Fig, 1D; Anova: vector effect: $F_{1,101}$=1.291, p>0.200)), however, the three visual conditions did (Fig, 1D; Anova: visual condition effect: $F_{2,101}$=83.663, p < 0.001; Post-hoc: F vs. U: p<0.001; F vs. D: p=0.016; U vs. D: p<0.001): oscillations were most regular in unfamiliar terrain, intermediate in familiar environment and least regular in the dark (Fig, 1D, E; mean±se: $U_{(FV+ZV)}$ =171±19; $F_{(FV+ZV)}$ =68±6; $D_{(FV+ZV)}$ =50±3). The effect of individuality is significant (p=0.015), indicating that some individuals show more regular oscillations than others, across conditions.

We then investigated whether our different conditions influenced the oscillations' frequencies (Figure 1D, x axis), which indicates how quick the turn alternation happens. Here again, the PI state had no observable effect (Wilcoxon test for repeated measures; F: FV vs. ZV p=0.635; U: FV vs. ZV p=0.343, mean±se in F: FV=0.38±0.05 Hz, ZV=0.34±0.04 Hz; U: FV=0.19±0.01Hz, ZV=0.18±0.0009 Hz, Fig 1 D), however, independent of the PI state, the

oscillatory frequencies were significantly higher in a familiar (F) than in an unfamiliar (U) visual panorama ($p=0.023$, mean±se: $F_{(FV+ZV)} = 0.37 \pm 0.036$ Hz; $U_{(FV+ZV)} = 0.19 \pm 0.008$ Hz; Figure 1D). Thus, the presence of familiar visual cues tends to increase the frequency of oscillations.

In the dark however, peak magnitudes are significantly weaker, closer to Gaussian noise and with a wider frequency range, suggesting that the PSD peak in some individuals may result from noise (Figure 1D, E). Oscillations seems to persist in the dark, however their expression is greatly inhibited suggesting that visual input is important for the expression of oscillation (Figure2).

Overall, these results confirm the existence of regular oscillations and that their expression are influenced by the perceived familiarity of the visual surrounding, with slower and most regular oscillations being expressed in unfamiliar terrain (Figures 1D, E, S4A). The second ant species *I. purpureus* showed significantly regular oscillations, too, with the same tendency to produce slower oscillation in visually unfamiliar terrain and to inhibit their expression when in the dark (Figure S3).

The navigational context modulates the angular and forward velocity of oscillations

To investigate the dynamics of the ant oscillatory movements in more details, we combined for each ant its body angular velocity signal – obtained from video recording – with the forward movement signal – obtained from the trackball movements. We reconstructed 'average cycles' for each individual by pooling the angular and forward velocity recordings 3s before and 3s after the moments when ants switch from a left to a right turn (i.e., when the time series of the angular velocity crosses zero from negative to positive; see Figure S5). That

way, we can quantify each individual's average dynamic of angular and forward velocity and compare them across conditions.

The visual surrounding had a strong effect ($p<0.001$): ants displayed higher peak of angular velocities (Figure 3B, upper row; mean±se: $U_{(FV+ZV)}$=129±4.8 deg/s; $F_{(FV+ZV)}$=67.5±4.4 deg/s) and higher forward velocities amplitude (Figure 3B, second row, mean±se: $U_{(FV+ZV)}$=4.8±0.34 cm/s; $F_{(FV+ZV)}$=2.3± 0.2 cm/s) in an unfamiliar environment. There was however neither an effect of the PI state on turn or forward velocity ($p>0.05$) nor an interaction between the visual surrounding and the PI state (mean peak of angular velocity model: AIC=160.9, interaction $p>0.05$; amplitude of forward velocity model: AIC=109.9, interaction $p=0.22$). Therefore, the amplitude of lateral oscillations within the path are larger in an unfamiliar panorama than in a familiar one, independently of the PI sate (Figure 1E).

Lateral oscillations are combined with specific forward velocities variations.

To test for the existence of conserved oscillatory dynamics across individuals, each individual average cycle (Figure S2 F-I for method example) was normalised and averaged to obtain a cycle at the population level. To ensure that we pooled ants oscillating at similar frequency ranges, we separated data from familiar and unfamiliar terrain and selected only individuals showing a peak frequency within 0.1 to 0.27 Hz for *M. croslandi* (N=12). These frequency ranges correspond to high magnitude, ensuring that they are not a consequence of noise. The emerging population-averaged oscillation patterns show the existence of movement dynamics that are consistent across individuals, for both familiar and unfamiliar environments (Figure 2 A). Forward velocity co-varies with angular velocity in a particular way. Forward velocity is quite low when the ants reverse their turning direction (i.e., when

angular velocity crosses zero). In contrast, we observe significant peaks of forward velocity, which happen briefly (up to 1s) while the ant is sweeping to the left or right (Figure 2A). Remarkably, these peaks coincide well with the moment when the ants' body orientation is aligned with its overall direction of travel (Figure 2A, dashed lines) even though during these moments the ants' angular velocity is quite high. The same covariation is present in our second species *I. purpureus* (Fig S3C, D), showing that this signature is not a specificity of *M. croslandi*.

We replicated the same analysis using tracks of *M. croslandi* ants recorded directly on the ground while displaying learning walks around their nest and observed the same relationship between forward and angular speed (Figure S4), which confirms that these dynamics are not a consequence of being mounted on the trackball set-up.

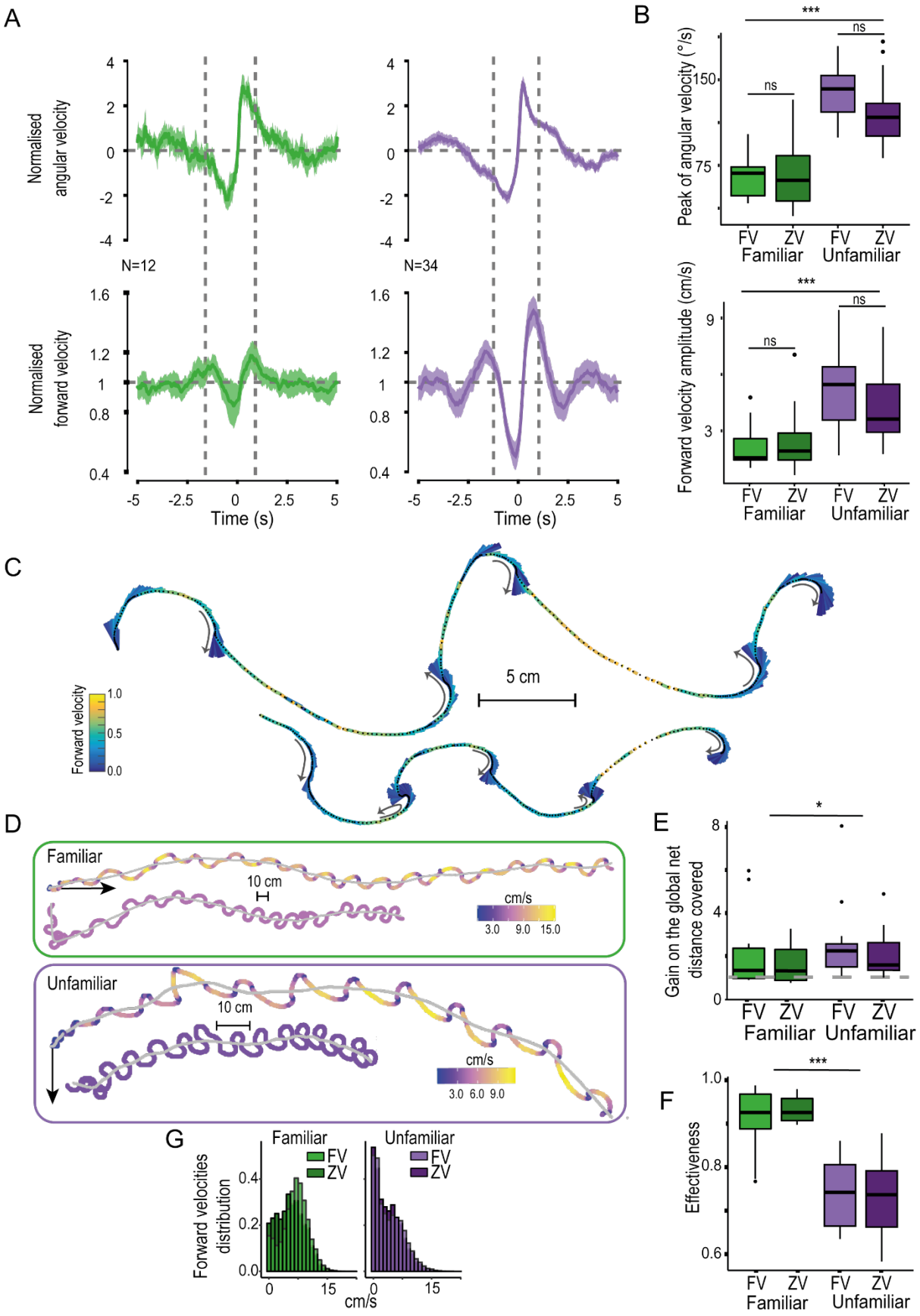

Figure 2: Co-variation of forward velocity and angular velocities optimize the distance covered and visual exploration. (A) Angular velocities (top-row) and forward velocity

(bottom row) co-vary in a way that seem conserved across visual condition (on familiar route (green) or in unfamiliar terrain (purple)). Population cycles have been reconstructed by merging full- (FV) and zero-vector (ZV) data and normalising the data amplitude within the individual's average cycle (Figure S2 F-I). Colour areas around the mean curves represent the 95% confidence interval, based on the inter-individual variation. Dashed lines represent the moment when the ants are facing their overall direction of travels. (B) boxplots show the actual distribution of the non-normalised mean peak of angular speed (top row) and forward velocity amplitude (bottom row) for the individuals' average cycle (FV on the left, ZV on the right). (C) Details of paths (12s) displayed by two different individuals in unfamiliar terrain. Black dots indicate the successive positions of the animal and vectors indicate the current heading direction. Variation of forward velocities are indicated by both the colour and the length of the vectors (the longer the vector, the smaller the forward speed and thus the higher the time spent in this direction). Grey arrows emphasise the directions of turns. (D) Reconstructed path (100s) of two individuals recorded in a familiar (green panel) and in an unfamiliar (purple panel) panorama. Each path has been either reconstructed with the actual forward velocity signal of the ant (top path) or with a constant speed (mean of the individual's forward velocity signal, bottom path). Colour scales indicate the forward velocity. For each path, the global trajectory is shown in grey (i.e., path smoothed to remove the lateral oscillations). Straight black arrows indicate the direction of the nest. (E-G) Population statistics across conditions. (E) Ratio of the effective distance covered (length of grey path in (D)) between the reconstructed path with variation speed against path with constant speed for the different condition. A ratio >1 (dashed grey line) indicates that the effective distance covered is longer with forward speed variation than without. (F) Ratio between the effective distance covered (length of grey path in (D)) and the actual distance walked. (G) Distribution of the forward velocity in cm/s for each condition.

Thus, ants (Figure 2, S4, S3) display large sweeps from one side to the other and thus spend a minimal amount of time facing their goal direction (i.e. the middle of the sweep), as angular speed is high at this moment. However, they produce a burst of forward velocity during this moment, that is, when aligned with their direction of travel (Figure 2A, C, D). On the contrary, they slow down, sometimes up to a pause, at the end of each left and right sweep, that is, when their body is facing away from their overall direction of travel (Figure 2A, C, D, G).

The dynamics of lateral oscillations optimise the distance covered.

311 To investigate the benefit of such regular variations of forward movements within the
312 oscillations' cycle, we compared the ant's real paths with reconstructed versions of their path
313 where we kept the original angular speed signal but averaged the forward speed, so it became
314 constant (Figure 2D). By doing so the actual distance walked remains identical, but
315 remarkably, the effective ground distance covered (length of the grey paths in Figure 2D) by
316 the original paths (with forward speed variation) increased by up to a factor 8 (median =1.5;
317 25 / 75 percentiles = 1.08 / 2.5) compared to the paths with constant speed. This positive gain
318 concerns 81% of our individuals and is significant in all our conditions (ratio above 1:
319 ps<0.009, Figure 2E).
320 We then looked at the ratio between the effective ground distance covered (length of the grey
321 path in Figure 2F) and the actual distance walked across conditions. The smaller the ratio the
322 more local oscillations are impeding the ants to cover effective ground (a ratio of 1 indicates
323 a straight path, without local oscillations). Such an 'effectiveness ratio' is impacted by the
324 presence of familiar visual surrounding but not by the PI state (panorama effect:
325 $F_{1,101}$=142.090, p < 0.001; PI effect: $F_{1,101}$=0.683, p = 0.407). Paths displayed when on
326 familiar terrain are more effective to cover ground than in an unfamiliar environment (Post-
327 hoc, Figure 4D, F vs. U: p<0.001). This is in line with the fact that ants displayed smaller
328 amplitude of oscillation in the presence of a familiar panorama (Fig 2A, B). In addition, we
329 observed that ants in familiar environment displayed less pauses (Fig 2G) and higher forward
330 velocities (N =34, p < 0.001, mean±se: F =6.087±0.336, U=3.961±0.182 cm/s).
331
332 **Oscillations are modulated by rotational feedback**
333 To test whether oscillations result from an intrinsic oscillator rather than a control mechanism
334 based on an external directional reference (i.e., servo-mechanism), we investigated whether
335 ants deprived of rotational feedback (either via optic-flow or compass cues) would still

oscillate. To do so, ants were mounted on the trackball in a way that prevented them from physically rotating their body on the ball: when the ant tries to turn, it is the ball that counterturns. In other words, the fixed ant experiences neither a change of body orientation nor visual rotational feedback when trying to turn (see Figure S2B). For this experiment, we recorded *M. croslandi* ants in unfamiliar terrain as this condition produced the clearest oscillations in our previous experiments (Figure 1D). To control for potential effects of facing directions (depending on celestial or terrestrial visual cues), we tested each ant fixed in eight subsequent different orientations with a 45° rotational shift.

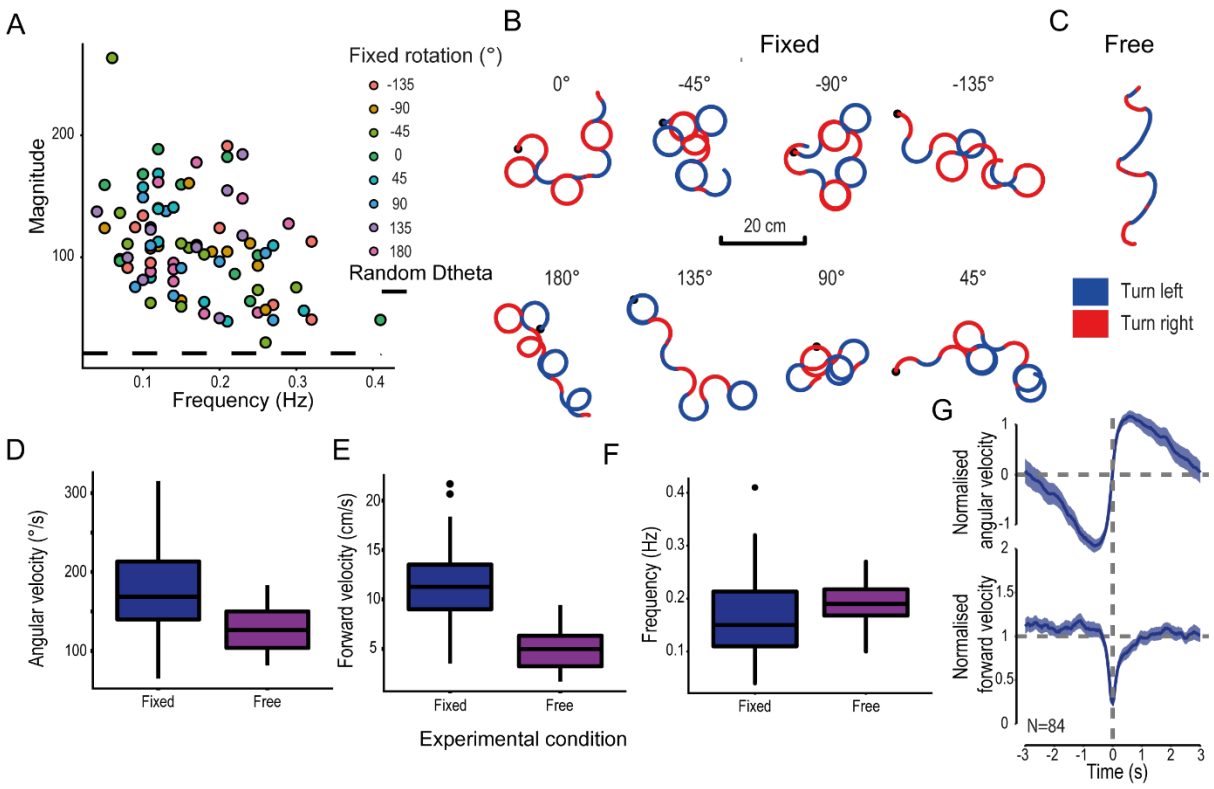

Figure 3. Ants still oscillate in the absence of rotational feedback. Zero-vector ants were tethered on the trackball in a way that prevented actual body rotation and tested in an unfamiliar environment. (A) Distribution of the individual Fourier dominant peak frequency and magnitude based on the angular velocity's spectral density time series (as in Figure 1D), method see Figure S2 B, C, D, E). High frequency indicates a fast-oscillatory rhythm, and a high magnitude indicates a strong presence of this oscillatory rhythm. The colour symbols represent the rotation relative to the theoretical nest direction (0°). The dashed black line represents the mean magnitude obtained from 200 Gaussian white noise signals (18.75). (B)

Example paths of different individuals fixed in different orientations. (C) Example path from an ant that was free to rotate on the trackball, recorded in unfamiliar terrain in previous experiments. (B, C) In both situations, ants alternate regularly between right (blue) and left (red), but turns are sharper in the absence of rotational feedback. Peak of angular velocity (D), peak of forward velocity (E) and Frequency (F) of the individual's average oscillation cycle show that ants move faster, turn faster and slightly longer in the absence of rotation feedback. (G) Angular velocities (top-row) and forward velocities (bottom row) co-vary in a way that seem conserved across experimental conditions. Population cycles have been reconstructed by merging all rotational condition as there is no differences of amplitude of mean peak of angular velocity and mean forward amplitude cycles between rotational conditions (Anova: Df= $F_{7,84}$= 1.0103, $p \geq 0.432$). Each individual signal has been normalised before pooling. Coloured areas around mean curves represent the 95% confidence interval, based on the inter-individual variation.

Despite the absence of visual rotational feedback, the obtained peak magnitudes of the angular velocity power spectral density (PSD: see Star Method) were much higher than expected from a Gaussian white noise ($p<0.001$) clearly showing the presence of a regular alternation between left and right turns (Figure 3A, B). The ants' body orientation relative to the world had no effect on the magnitudes (orientation: $F_{7,83}=0.3729$, $p=0.914$) nor did the other random parameters (individual $p=0.933$, sequence $p=0.473$). The mean oscillation frequencies (mean±se: 0.17±0.007 Hz) were quite close to what we observed when these ants were free to rotate in an unfamiliar environment (Wilcoxon test for repeated measures: $p=1$, $N=88$, Figure 3F). Thus, ants can display regular turning oscillations without rotational feedback, whether as a result of optic flow or a change of orientation relative to directional cues such as the visual panorama, wind, celestial compass cues or the magnetic field. Here again, the lateral oscillations displayed by the fixed ants showed the simultaneous variation of forward speed, as observed in the other conditions (Figure 3G). Consequently, we are left with the conclusion that these oscillatory dynamics are generated intrinsically.

Interestingly, the absence of rotational feedback led to higher angular velocities (mean: fixed=176 deg/s; free=128 deg/s; $p<0.001$), higher forward velocity (mean: fixed=11 cm/s; free=5 cm/s; $p<0.001$) and slightly slower turn alternation (i.e., lower frequency: fixed=0.16

Hz; free=0.19 Hz, p=0.0189) than ants that were free to physically rotate on the ball (Figure 3A-F). Rotational sensory feedback is thus involved in limiting the amplitude of the oscillations.

The observed movement signature emerges readily from a simple neural circuit.

Similarly to previous work[44,45], we designed a simplistic neural model based on the circuitry of the insect pre-motor area so-called lateral accessory lobes (LAL). The purpose of this model was not to match observed data quantitatively[20] but simply to test whether the co-varying relationship observed between angular and forward velocity could emerge from this type of circuit. Activation of the neurons in the left and right pre-motor areas are known to mediate left and right turns respectively in insects[11,13,45–48]. Furthermore, these left and right regions are known to reciprocally inhibit each other[11,13,45,47]. Modelling two reciprocally inhibiting neurons with internal feedback – that tries to maintain a basal activity – is sufficient to obtain the typical oscillatory activity between left and right LAL[11,45] (Figure 4) and thus provides an explanation for the regular oscillations between left and right turns observed in insects. Interestingly, we show here that simply assuming that forward velocity is controlled by the sum of left and right output – while angular velocity results from their difference[14,20,45]– is sufficient for the covariation observed in ants to emerge (Figure 4). Bursts of forward speed appear when one side largely dominates over the other, that is when the ant is at the maximum speed of its angular sweep and thus roughly aligned with its overall direction of travel. Inversely, a break of forward speed occurs when the dominancy is reverted between LAL neurons, that is at the moment where ant reverts their turning direction (Figure 4). Importantly, the emergence of this particular relationship is robust to parameter change (Figure S5) and thus a stable feature of these types of circuits.

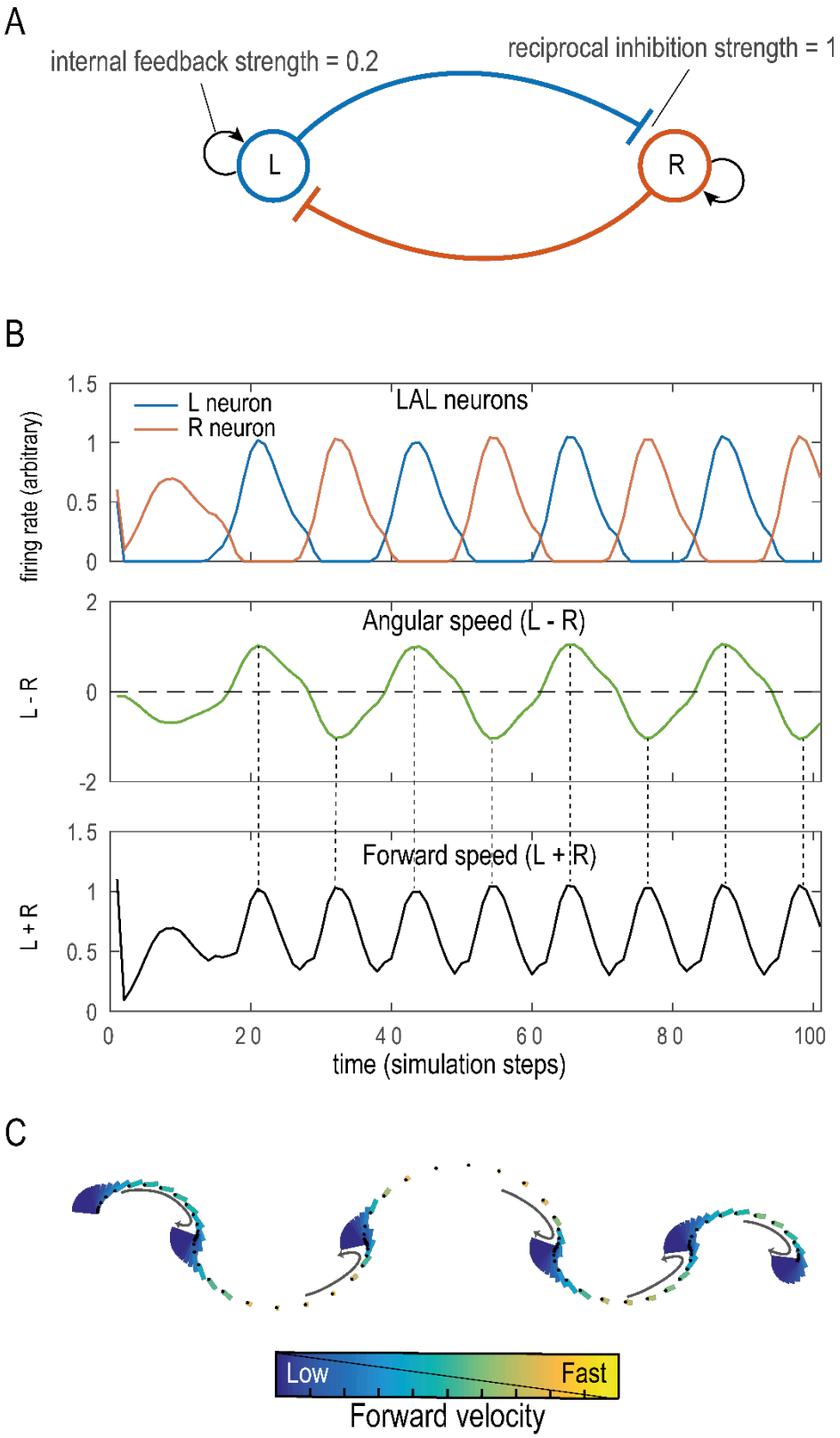

Figure 4. Reciprocal inhibition between two units produces the observed relationship between angular and forward velocity.

(A) Scheme of the model abstracted from the lateral accessory lobe (LAL). The Right (R) and Left (L) hemisphere neurons reciprocally inhibit each other (blue and red connection), while trying to sustain a basal firing rate through internal feedback (black arrow). (B) This results in

the emergence of stable anti-phasic oscillatory activity between the R and L neurons (B, upper row). Assuming that angular velocity is controlled by the difference (B, middle row) – and forward speed by the sum (B, bottom row) – between left and right activation is sufficient to elicit the movement dynamics observed in ants (compare Figure 4C with Figure 2C). (C) Details of the dynamic of the path generated by the model. Colour indicates forward velocity (scales are arbitrary). Black dots indicate the successive positions of the agent and vectors indicate the current heading direction. Variation of forward velocities are indicated by both the colour and the length of the vectors (the longer the vector, the smaller the forward speed and thus the higher the time spent in this direction). As ants, the model results in a zigzagging path where velocity drops during turn reversal and increases when facing the overall direction of travel (Figure 2A, C, D). While the model enables the modulation of amplitude and frequency of the oscillations, the forward/angular velocities relationship is quite robust to parameter change (Figure S5).

Discussion

An embedded solution for the compromise between exploration/exploitation

We recorded the detailed locomotor movements of two distantly related ant species – *M. croslandi* and *I. purpureus* – using a trackball-treadmill device directly in their natural environment. Despite that one species is a solitary visual navigator (*M. croslandi*) and the other (*I. purpureus*) uses pheromone trails and mass recruitment, we noticed a remarkable similar behavioural signature. Both species continuously display regular lateral oscillations with a synchronised burst of forward speed when facing the general direction of travel (Figure 1, 2A, C, S3). This pattern movement strongly optimises the overall ground distance covered while simultaneously enabling the ant to slow down when scanning to left and right directions, which may extend up to a full U-turn in some ants (Fig 2 C-F).

Previous observations assumed that ants accelerate when facing their goal direction as a response to the recognition of familiar views when aligned in this particular direction[49–51]. Here we show that this acceleration is the product of an endogenous process, as it is still expressed in unfamiliar terrain or when the ant body is artificially fixed on our trackball in a given

452 orientation (Figure 3). This findings stresses the often disregarded importance of internally
453 generated movement within the 'sensorimotor' loop[2,8,52–54].
454
455 The described internally generated movement dynamic provides an embedded solution for the
456 compromise between exploration (looking on the side) and exploitation (covering ground in
457 the desired direction). External visual cues can then modulate the exploration/exploitation
458 balance to the task at hand by simply adjusting the amplitude of this endogenous dynamic.
459 Higher amplitude oscillations optimise 'exploration' (higher amplitude scans) in an unfamiliar
460 environment, while lower amplitudes favour 'exploitation' (straighter paths) on a familiar route
461 (Fig 2, S3).
462 Interestingly, this movement signature is equally useful, and used, during the acquisition of
463 learnt visual information, when naïve ants display their learning walk around the nest[27] (Fig
464 S4). Optimising the learning of visual cues in naïve ants requires to bias the balance towards
465 'exploration' in the same manner as searching for familiar cues in an unfamiliar environment
466 does in experienced ants; thus, it is not surprising to see here also high amplitude oscillations
467 (Figure 2A-D, S3). The apparent different needs for the acquisition of information on the one
468 hand and the use of that information on the other hand, are thus solved with the same sensory-
469 motor solution. The weaker modulation observed in *I. purpureus* (Figure S3) may be explained
470 by their strong reliance on chemical trails[35], whose absence on the trackball may favour
471 exploration in both visually familiar and unfamiliar conditions.
472 Finally, we see in both species that the internally generated oscillations can be strongly
473 inhibited when not needed, such as when moving in the dark (Figure 1C, D, S3A, B). Indeed,
474 oscillations are not always useful and it may be advantageous to repress them in situations like
475 when inside the nest or when trying to escape an aversive situation. Thus, both the animal's
476 internal state and the presence/absence of relevant contextual information – such as a visual

panorama by opposition to no panorama at all – modulates the expression of the internally produced oscillations in a similar vein as the male fly's internal state continuously tunes up or down the gain of circuits promoting visual pursuit[55]. However, what specific type of visual information promotes the expression of oscillations remains to be seen.

Evolutionary consideration and neural Implementation.

Lateral oscillations around 0.3-1Hz are also observed in moths[12,15,16,56] *Drosophila* larvae[14], Colorado beetles[42], flying hymenopteran[29,30,57] and other insects[13], suggesting an ancestral way of moving, which predates at least the holometabolous insects' common ancestor (around 300 Myr ago).

In the insect brain, regular lateral oscillations seem to result from reciprocal contra-lateral inhibitions between left and right hemispheric premotor areas, so-called Lateral Accessory Lobes (LAL) an ancestral brain structure, highly conserved across insects[13,44,45]. These circuits – analogous to central pattern generators (CPG) – result in the internal production of asymmetrical and rhythmical excitation between left and right motor commands, so-called flip-flop neurons[11,13,45–48]. However, while CPG are well known to sustain a wide range of rhythmical limb movements[8,53,58,59], the LAL controls the displacement of the whole animal across space and thus directly contributes to the navigational task.

Some have suggested that neural systems evolved at first to coordinate movements endogenously[54,60] whereas the modulation of these movements by external sensory information originated only as a second step[60]. This view is supported by the current demonstration of an internally produced rhythm at the core of the navigational behaviour in ants, as well as the observation that, across species, various multi-modal sensory cue converge to the same conserved region (the LAL) to produce the remarkable variety of navigational behaviours across species[13,17,44,45]. Modulation of oscillations by olfactory cues

503 helps *Drosophila* larvae[14] to climb odour gradient, male moths to track pheromone
504 plume[12,13,15–17] and ants to follow chemical trails[18]. Modulation of oscillations by vision for
505 navigation, as observed in wasps[29,30] bumblebees[31] and ants[23–28] may have appeared later
506 with the evolution of visual navigation in hymenopteran, through direct or indirect
507 connections between the mushroom bodies – the seat of navigational visual memories[50,61,62]
508 – and the LAL (Figure 4). Modulation of oscillations by re-afferent rotational visual cues, as
509 we showed here in ants (Figure 3), might be ancestral to insects as we equally observe it in
510 moths[16,17,63]. This likely evolved through connections between horizontal optic-flow detectors
511 in the optic lobes[16,64] and the LAL (Figure 4), providing a useful feedback-control to calibrate
512 the amplitude of turns, and more generally participating in the widespread opto-motor
513 response[16].
514
515 The forward speed variation within the oscillation cycles presented here has not been
516 reported in other insects' species and the fact that it is shared in two phylogenetically and
517 ecologically distant ants (Fig S3) suggests that it is a shared feature in the ant family. This
518 may be an adaptation for the use of vision while walking. Scanning multiple direction
519 through body rotation is key for visual scene recognition in hymenopteran[40,65,66], and because
520 ants are ground dwellers, they are reluctant to decouple their body orientation from their
521 direction of travel; even though they can[67]. Ants thus benefit to pause when looking on the
522 side, otherwise they would depart away from their general direction of travel. Conversely, the
523 timely burst of forward speed when facing the overall direction of travel (Fig 2A, C, D)
524 enables to stretch the oscillations and thus strongly improves the amount of ground covered
525 (Fig 2 D-F). In addition, pausing when looking on the side must improve the efficiency of
526 visual recognition due to gaze stabilization, which accommodates remarkably well the idea

that views are learnt and recognized when oriented left and right – rather than towards and away – from the goal[29,68].

Interestingly, the efficient covariation between forward and angular velocity observed here in ants is captured by a model of the LAL by simply assuming that forward speed results from the summed excitation of both hemisphere motor commands; while turning velocities results from the difference between left and right excitation (Figure 4). Certainly, we do not exclude that more complex circuitry could produce other regimes of covariations, but our simple model shows that this particular relationship between forward and angular speed is robust to parameter change (Figure S5), and thus can readily emerge from the LAL. However, the oscillations' amplitude and frequencies vary with parameter change, at least across a factor of 2 (Figure S5). Therefore, we can easily envision how various inputs into the LAL (such as pictured in Figure 5) could modulate the amplitude and frequency of the emerging oscillations, without altering the fundamental relationship between forward and angular velocities. For instance, inputs from the central complex such as PFL2 neurons project bilaterally to the LAL[69–71] and could thus promote the overall modulation of oscillations amplitude as shown here. Inversely, PFL3 neurons, which project unilaterally to the LAL, could mediate lateralised information, whether from memorised views [68] or path integration[72,73] to bias the oscillations toward one side[71]. Understanding precisely how such inputs interact with oscillations in insects opens the door to a complexity that would be too vast to tackle here, but given the rapid development of neurobiological tools and knowledge about the circuitry of the lateral accessory lobes, this may constitute a realistic endeavour in the near future.

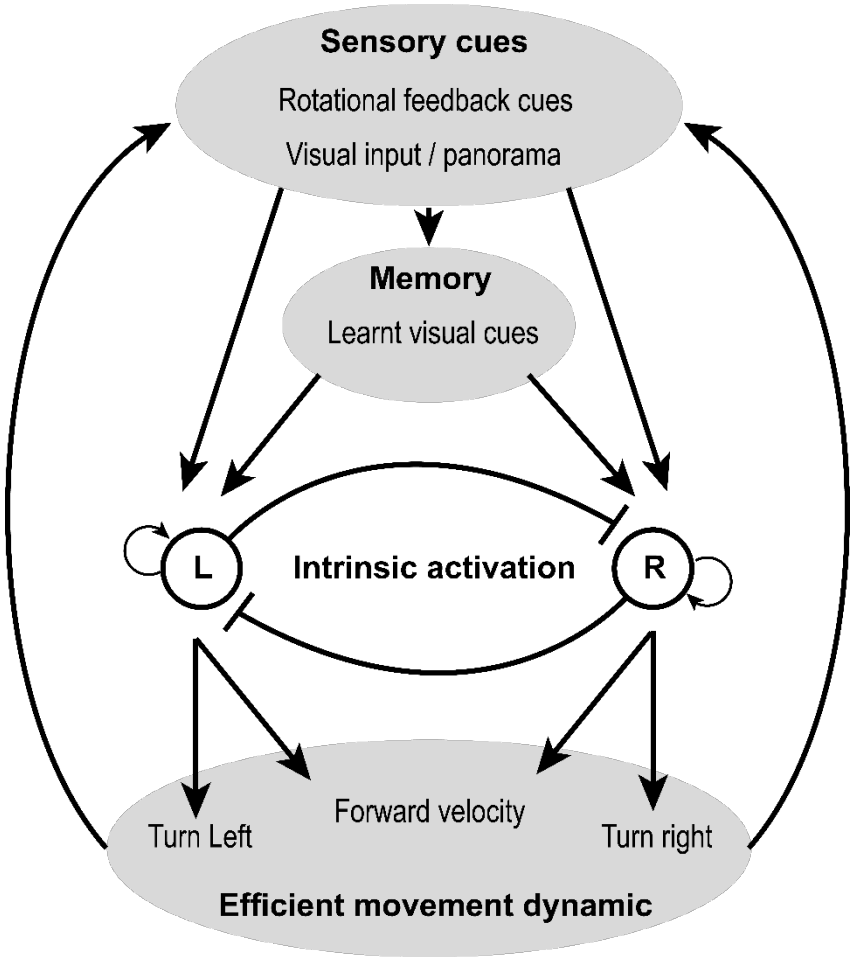

Figure 5. An intrinsic oscillator at the core of visual navigation.

We propose a simple scheme to encompass our results. In this view, sensory input (in this case various innate and learnt visual information) act on behaviour only indirectly, through the systematic modulation of an intrinsic oscillator. The latter ensures that an efficient movement dynamic is preserved across navigational contexts, which would not necessarily be the case if various and potentially conflicting sensory information were directly modulating movement. This scheme also highlights the idea that action is not merely the product of perception. At the core of behaviour lies an intrinsic, self-generated dynamic, which are modulated, rather than controlled, by sensory perception.

STAR methods

RESOURCE AVAILABILITY :

Lead contact

Further information and requests for resources and reagents should be directed to and will be fulfilled by the lead contact, Leo Clement (clement.leo@univ-tlse3.fr).

Materials availability

As experiments took place in the natural environment this study did not generate new unique reagents.

Data and code availability

Any data or code information required to generate this results paper is available from the lead contact upon request.

- All data reported in this paper will be shared by the lead contact upon request
- All original code has been deposited at: https://github.com/awystrac/Neural_oscillator and is publicly available as of the date of publication.
- Any additional information required to reanalyze the data reported in this paper is available from the lead contact upon request

EXPERIMENTAL MODEL AND SUBJECT DETAILS

Study Animal & Experimental site

All experiments took place within an open grassy woodland at the National Australian University, Canberra from Feb. to Mar. 2019. We had the opportunity to work with two Australian endemic ant species: *Myrmecia croslandi* and *Iridomyrmex purpureus*. *Myrmecia croslandi* workers are known to forage solitarily, with each individual either hunting on the ground in the vicinity of the nest or navigating routinely back and forth toward the same favorite foraging tree throughout her life span[66]. These ants rely mainly on learnt terrestrial visual cues to navigate but are also able to resort to PI when the visual environment does not provide guidance[27,32,39,66]. Eight nests of *M. croslandi*, that foraged on two distinct trees between 6.0 and 30.0 m away from the colony, were used in this study. *Iridomyrmex purpureus* ants form large colonies and forage along pheromone trails that lead to food patches. Despite employing pheromone trails for recruitment, this species also uses both learnt visual information and path integration for navigation[31]. We also performed navigational experiments with two *I. purpureus* nests to ensure that this species relies indeed on both learnt visual terrestrial cues and path integration, which they did surprisingly well (see Figure S1). For the main experiment, a feeder was placed 7.0 m away from the nest and foragers were free to familiarize themselves with the route for 72 h before being tested.

METHOD DETAILS

Trackball system and data extraction

During tests, ants were mounted on a trackball device[38]. This device consists of a polystyrene ball held in levitation in an aluminum cup by an air flow. The trackball has two sensors placed at 90° to the azimuth of the sphere, which record the movements of this sphere and

translate them into X and Y data retracing the path of the ant. The X and Y acquisition of the trackball rotations happened at a 30 Hz frequency (i.e., 30 data points per second), enabling us to reconstruct the ant's movements with high precision. Additionally, a camera (640×480 pixels) recording from above provided details of the ant's body orientation, also at 30 Hz. We also analyzed *M. croslandi* learning walks recorded directly on the natural ground. Head directions were obtained via video recordings at 25 Hz (provided by Jochen Zeil).

In this study, we used two different trackball configurations to record the ants' motor responses: further referred to as 'Free ant' and 'Fixed ant' experiments, respectively.

Free ant experiments: two small wheels prevented the polystyrene ball from rotating in the horizontal plane, however, all other degrees of freedom of the ball rotation were accessible (Figure S2 A; 'closed-loop'[38]). Ants were attached on top of the ball by putting magnetic paint on their thorax and a micro-magnet fixed at the bottom end of a single dental thread that was in turn attached to a 0. 5 mm pin. Crucially, the pin was placed within a glass capillary. This procedure enabled the ants to execute physical rotations on the ball (the ball is not rotating horizontally) but prevented any translational movement. Ants could thus execute body rotations and control the direction in which they faced but any attempt to go forward or backward resulted in ball rotations. We used the recorded videos to manually track the ants' body orientation through time using the free software Kinovea (v-0.9.1).

Fixed ant experiment: the two small wheels were no longer in place. Hence, the ball could now turn in any direction, including the horizontal plane (Figure S2B; 'open-loop'[38]). Ants were tethered directly to a needle with a micro magnet (glued at the end of the needle) and magnetic paint on their thorax. The top end of the needle was glued to a small piece of paper sheet (0.5×2.5 cm). Consequently, the fixed ant could no longer rotate, and the experimenter could choose in which direction individual was facing. Any attempt to move,

including turning, by the ants resulted in ball rotations. This trackball configuration was only conducted with the more robust *M. croslandi*.

Free ant experiments: protocol

At the start of each test, the ant was mounted on the trackball device but surrounded by an opaque cylinder (30×30 cm) that prevented the ant from seeing any cues from the visual scenery around her. Once the ant was in place on the device, the whole apparatus was moved to the desired test location in the field. Afterward, the surrounding cylinder was removed, revealing the visual scenery to the ant and data recording began. To ensure a high level of homing motivation, only individuals who had previously received a 40% sucrose solution (for *M. croslandi*) or a food item (for *I. purpureus*) were tested. The recording period was 3.5 min for the robust *M. croslandi* and 1.5 min for the flimsier *I. purpureus*.

To test the impact of terrestrial visual cues on the oscillation behavior, ants were tested under three distinct conditions.

Familiar (F): ants were tested along their habitual route, which therefore presents a familiar visual view.

Unfamiliar (U): ants were tested at least 50 m away from the habitual route, which therefore presents an unfamiliar panorama.

Dark (D): ants were tested in total darkness, within an opaque cylinder (30×30 cm) covered with a red Plexiglas plate that transmitted only the low red wavelengths, which ants cannot perceive[67,68].

To test the impact of PI on oscillation behavior, ants were tested as either full- or zero vector ants. Full vector (FV): ants were caught at the start of their inbound trip to the nest

(i.e., at the foraging tree for *M. croslandi* and at the feeder for *I. purpureus*). FV ants have an informative homing PI vector, which points in the food-to-nest compass direction. Consequently, FV ants can rely on both PI vector and the learnt visual scenery while being tested. Zero vector (ZV): homing ants were captured just before entering the nest, that is, at the end of their inbound trip. Hence, their PI homing vector is reduced to zero and thus no longer directionally informative. Consequently, ZV ants can only rely on the learnt visual scenery while being tested. For each of the three visual conditions FV and ZV ants were tested, resulting in a total of six conditions.

For *I. purpureus*, at least 16 ants were tested in each of the six conditions (F: FV&ZV =16; U: FV&ZV =17; D: FV=16 & ZV=17). Since *I. purpureus* forms very populous colonies with an abundance of foragers, all individuals were tested only once, in one of the six conditions. The data obtained are therefore statistically independent. On the contrary, *M. croslandi* forms sparsely populated colonies and individuals usually make only one foraging trip per day[66]. Thus, it is time-consuming and challenging to capture, mark and follow individuals throughout foraging trips. Individuals were therefore captured (either at the foraging tree (FV) or before reaching their nest (ZV)) and tested successively in a pseudo-random order in all three visual panoramas: Familiar (F), Unfamiliar (U) and in the Dark (D). Both the sequence in which the visual conditions were experienced and the individuality were included in the statistical models as it is likely that the state of the PI vector will be modified across successive tests. Overall, 32 *M. croslandi* ants were tested with some individuals tested as ZV or FV ants on two different days. At least 16 *M. croslandi* ants were tested in each of the six conditions (F: FV&ZV =17; U: FV&ZV =17; D: FV=17 & ZV =16). Overall, 101 recordings were obtained.

In the ‘free ant’ experiments, the ant’s body axis can turn without the ball movement. We used the recorded videos to manually track the ants’ body orientation through time using

683 the free software Kinovea. We removed the first 3s of recording of each ant as the removal of
684 the opaque ring may have disrupted the behavior. Overall, the analyzed recording length was
685 100s (except for two ants: 84 and 99s) for *M. croslandi* individuals and 50s (except for two
686 ants: 49s) for *I. purpureus* ants. For details of the Fourier analysis (see below); nine paths of
687 *I. purpureus* were discarded (F FV=1, U FV = 1, U ZV =2, D FV =2, D ZV = 3) as the ants
688 displayed too many pauses.

689

690 **Fixed ant experiments: protocol**

691 To test if oscillations are due to an intrinsic oscillator or caused by the fact that ants try to
692 keep a bearing toward an external stimulus, we conducted an additional experiment on *M.*
693 *croslandi* ants. We recorded foragers without an informative integration vector (ZV) in the
694 same unfamiliar environment (U) as before. Ants were tested in eight different fixed
695 orientations, covering the 360° azimuth by bins of 45°; and with one direction corresponding
696 to the food-to-nest compass direction. Each ant was tested in all eight orientations in a
697 pseudo-random sequence. To change the ant's orientation, the experimenter would first place
698 the opaque cylinder (30×30 cm) around the trackball system to prevent the ant from
699 perceiving the visual panorama, then rotate the whole set-up (trackball and mounted ant) and
700 finally remove the opaque cylinder to re-start data collection. Ants were recorded for at least
701 15s up to 20s in each orientation. Eleven ants were tested in all eight orientations. Since the
702 ants were fixed, trackball rotations along the horizontal axis provided a direct measure of the
703 angular velocity of the attempted turn generated by the ant. Angular velocity time series were
704 then extracted from the trackball data. At the end, the available length of the recordings for
705 the analysis had 512 frames (~17s) except for 5 individuals (294,394,456,474,494 frames). It
706 should be noted here that prior to the Fourier analysis (see below) we added a series of 0s

(zero padding) at the end of the time series until it had a length of 3000 data points to match the same recording length obtained in the free ant experiment). This permits to increase the precision in the frequency range obtained from the Fourier analysis.

QUANTIFICATION AND STATISTICAL ANALYSIS

All statistical analyses have been run using the free software R (v 3.6.2. R Core Development Team). For all statistical tests, the p-values were compared to the critical alpha risk at 0.05, with the appropriate correction if needed. Statistical parameters mean and the associated standard error is given within the text and/or on figures: N represents the number of individuals.

Fourier analysis

To reveal the occurrence of regular lateral oscillations, we choose to focus on the angular velocity value (Figure S2C), which constitutes a direct reading from the left/right motor control. This time series was processed through three successive steps to obtain its 'spectral density', according to the Wiener-Khinchin theorem. First, the signal was parsimoniously smoothed with a moving median running of a length of five frames (0.17s) to reduce the influence of the recording noise (Figure S2D, dashed blue line). Then, the recorded time series was passed through an autocorrelation function (Figure S2D). Finally, a Fourier transform was performed on these autocorrelation coefficients, providing the power spectral density (Figure S2E). With this approach, the magnitudes obtained are independent from angular drift and amplitudes of the oscillations and thus can be directly compared across individuals. A high magnitude indicates a strong oscillation for a given frequency. For each individual, the dominant frequency (i.e., presenting the highest peak magnitude) and its magnitude were extracted (Figure S2E, dashed blue lines). To check whether these

magnitudes indicate a significant regular oscillation, we compared them to the average spectral density magnitude resulting from 200 Gaussian white noise signals of the same length (within each species and experiment). Gaussian white noise signals were obtained by drawing a sequence of random values drawn from a normal law. These simulated signals were then processed through the exact same operations as the ants' angular velocity recording: namely smoothing, autocorrelation, Fourier transformation and extraction of the highest peak magnitude. The mean of the 200 highest magnitudes obtained was then compared to the real ants' equivalent magnitudes with a Wilcoxon one-tail test. As each experimental group has been compared with this mean magnitude of the simulated angular velocity signal, the p-value is subsequently adjusted using the Bonferroni correction.

Average oscillatory cycle

To extract the average dynamics of an oscillation cycle, the mean cycles at the individual and population levels were reconstructed as follows. First, we smoothed the angular velocity time series of each individual by running twice a median with a window length of 31 frames for *M. croslandi* (for both free and fixed experiments), 25 frames for data during learning walks on the natural ground and seven frames for *I. purpureus*. This window length is much smaller than one oscillatory cycle and thus smoothens the data without altering the cycle general dynamics (Figure S2 F). Second, we indexed moments when the time series crosses 0 (from – to +) as t_0; and extracted a window of ±90 frames around the t_0 indices (±60 frames for *I. purpureus*; Figure S2 F). We then reconstructed a mean cycle for each individual by averaging the individual's extracted windows, aligned at t_0 (Figure S2 G). The individuals' average forward speed dynamics during one cycle was obtained in the same way by using the same indices t_0 obtained from the angular velocity data (Figure S2 H). For each ant, the mean

angular velocity peak and amplitude of forward velocity cycles were extracted for analysis. Finally, we reconstructed the average cycle at the level of the population by averaging the mean cycle of all individuals. Note that to do so, each individual's mean cycle was first normalized to show similar amplitudes (mean_cycle_normalised = mean_cycle/mean|mean_cycle_values|). The goal was here to observe the cycle dynamics through time and not to estimate the inter-individual variation in amplitude, which was analyzed previously using the individual's mean cycle amplitude. Note that the criterion used to align the time series (the change from a left to a right turn) necessarily creates an artefact in the averaged angular velocity obtained. Namely, an average change from left turn to right turn at t_0. However, several factors indicate the relevance of such pooling at the population level: (1) the period of the average cycle corresponds to the mean frequency obtained from the Fourier transform. (2) we can observe a significant reversal of the angular velocity before and after the mean oscillation cycle. (3) the associated forward velocities co-vary in a significant way, indicating the existence of conserved dynamics.

Analysis of the ants' direction of movement

We reconstructed the ant paths of time that derived from the trackball recording for a fixed period to determine the mean direction of movement (mu) as well as the mean circular vector length (r, a measure of dispersion) of each individual. The mean directions (mu) were analyzed using a Rayleigh test (from R package: Circular) that also includes a theoretical direction (analogous to the V-test). To test whether the angular data are distributed uniformly as a null hypothesis or if they are oriented toward the theoretical direction of the nest as indicated by the state of the PI or the familiar panorama, the average vectors lengths (r) were

analyzed via a Wilcoxon-Mann-Whitney test with a Bonferroni correction for multiple testing.

Analysis of optimization

To investigate the benefit of variation of forward and angular velocities signal on the overall ground distance covered we reconstructed for each individual a fictive path where forward speed was maintained constant (we took the average forward speed, so that the total distance walked remain the same as in the original path). To estimate the overall ground distance covered for a given path, we computed a 'global trajectory' by smoothing the path with a sliding window, until effectively removing the oscillations component (Figure 4B grey paths). To estimate the actual benefit of variation of forward speed on the distance covered, we compared the length of the 'global trajectories' between the fictive path (with constant forward speed) and original path (Fig 2D, E). A ratio >1 mean that the original path covered more ground distance, and vice versa. Ratios were compared with Wilcoxon one-tail test to the threshold one.

To test for an effect of the familiarity and vector on the distance covered we calculated an 'Effectiveness ratio' for each individual as the ratio between the length of the 'global trajectory' / 'actual distance walked' on the original paths with oscillations (Figure 2D, F). To enable a fair comparison across individuals, we computed the "effectiveness ratio" on a 100s portion of paths, using an additive mixed model.

Statistical models

For the free ant experiment, two types of models were tested: the first considering the interaction between visual panorama and vector modalities, the second with simple additive effect. It should be noted here that in case of deviation of the residuals of these models from normality and or homoscedasticity, the response variables have been transformed. Only the model presenting the lowest Akaike information criterion was retained and subsequently analyzed via an analysis of variance (Anova), followed by a post-hoc analysis of Tukey's rank comparison. Finally, for *M. croslandi* whose individuals were tested across several conditions, the models are mixed models that controlled the sequence and the individuality effect as random variable. For some models, we removed the sequence effect because of a singularity problem of this factor (i.e., the information given by this variable is already contained in other variables). For fixed ant experiments (which were tested only as ZV ants in an unfamiliar environment), the model analyzed the effect of the condition of the subsequent rotations.

COMPUTATIONAL MODEL

The computational model presented in Figure 5 has been built and run using Matlab® R2016b. The code is open access and available at :

https://github.com/awystrac/Neural_oscillator

It is a step-based model (‘For loop’). Two neurons (Left and Right neurons) reciprocally inhibit each other, while trying to maintain a baseline activity through self-excitation and internal feedback.

Variable	Description

L	Left neuron activity
R	Right neuron activity
LNF	Left neuron internal feedback
RNF	Right neuron internal feedback

822

Parameters	Description
W	Reciprocal inhibition synaptic weight
Baseline	Firing rate of the oscillator neurons without any external modulation (default at 0.5)
Exhaust rate	Rate at which the negative internal feedback is modulated between each time step
Noise	Standard error of the normal distribution of the noise added to the activity of the neurons of the oscillator (default at 0.1)

823

824 Initialization

825 R_1= random (0to1)

826 L_1 = random (0to1)

827 $RNF_1 = 0$

828 $LNF_1 = 0$

829

830 At each time step

L and R neuron update their activity due to their self-excitation, internal feedback, inhibition from the other neuron, and noise.

$$L_{t+1} = L_t - LNF_t - (R_t \times W) + (random(-1\ to\ 1) \times noise)$$

$$R_{t+1} = R_t - RNF_t - (L_t \times W) + (random(-1\ to\ 1) \times noise)$$

Set a hard limit to the activity both neurons

$$LM_{t+1} = \begin{cases} L_{t+1} & if\ L_{t+1} > 0 \\ 0 & if\ L_{t+1} \leq 0 \end{cases} \qquad RM_{t+1} = \begin{cases} RM_{t+1} & if\ R_{t+1} > 0 \\ 0 & if\ R_{t+1} \leq 0 \end{cases}$$

Update the internal negative feedback for the left and right motor neurons. The internal feedback changes proportionally to the difference between its own activity and the neuron activity (relative to the baseline activity)

$$RNF_{t+1} = RNF_t + \text{Exhaust rate} \times (R_{t+1} - RNF_t - \text{Baseline})$$

$$LNF_{t+1} = LNF_t + \text{Exhaust rate} \times (L_{t+1} - LNF_t - \text{Baseline})$$

Computation of the angular and forward velocities

Angular_velocity = R - L

Foward_velocity = R + L

Acknowledgments

We want to thank the Australian National University and particularly Jochen Zeil, Zoltán Kócsi and Trevor Murray for their advice and technical support. We also thank Hansjürgen Dahmen for providing us with the trackball system and Ajay Narendra for his incredible knowledge about the local Australian ants. We are grateful to all these people for their helpful advice. We also thank Jochen Zeil, Paul Graham and Michael Mangan for their helpful feedback on the manuscript. Finally, we thank the ants tested in these experiments for their participation.

Additional information

Funding

Funder: European Research Council, Grant reference number: EMERG-ANT 759817,

Author: Antoine Wystrach

Author contributions

LC Conception and Design of experiment, Data collection, Analysis and interpretation of data, Drafting and revising the article. SS Conception and Design of experiment, Data collection, Drafting and revising the article. AW Conception and Design of experiment, Data collection, Analysis and interpretation of data, Drafting and revising the article, Supervision of project.

References

1. Dittmar, L., Stürzl, W., Baird, E., Boeddeker, N. & Egelhaaf, M. Goal seeking in honeybees: matching of optic flow snapshots? *Journal of Experimental Biology* **213**, 2913–2923 (2010).
2. Gomez-Marin, A., Stephens, G. J. & Louis, M. Active sampling and decision making in Drosophila chemotaxis. *Nat Commun* **2**, 441 (2011).
3. Lehrer, M. SMALL-SCALE NAVIGATION IN THE HONEYBEE: ACTIVE ACQUISITION OF VISUAL INFORMATION ABOUT THE GOAL. *The Journal of Experimental Biology* **199**, 253–261 (1996).
4. Dawkins, M. S. & Woodington, A. Pattern recognition and active vision in chickens. *Nature* **403**, 652–655 (2000).
5. Otero-Millan, J., Troncoso, X. G., Macknik, S. L., Serrano-Pedraza, I. & Martinez-Conde, S. Saccades and microsaccades during visual fixation, exploration, and search: Foundations for a common saccadic generator. *Journal of Vision* **8**, 21–21 (2008).
6. Wachowiak, M. All in a Sniff: Olfaction as a Model for Active Sensing. *Neuron* **71**, 962–973 (2011).
7. Wesson, D. W., Donahou, T. N., Johnson, M. O. & Wachowiak, M. Sniffing Behavior of Mice during Performance in Odor-Guided Tasks. *Chemical Senses* **33**, 581–596 (2008).
8. Wolf, S. *et al.* Sensorimotor computation underlying phototaxis in zebrafish. *Nat Commun* **8**, 651 (2017).
9. DeBose, J. L. & Nevitt, G. A. The use of Odors at Different Spatial Scales: Comparing Birds with Fish. *J Chem Ecol* **34**, 867–881 (2008).
10. Freas, C. A. & Cheng, K. The Basis of Navigation Across Species. *Annu. Rev. Psychol.* **73**, 217–241 (2022).
11. Iwano, M. *et al.* Neurons associated with the flip-flop activity in the lateral accessory lobe and ventral protocerebrum of the silkworm moth brain. *J. Comp. Neurol.* **518**, 366–388 (2010).

12. Kanzaki, R., Sugi, N. & Shibuya, T. Self-generated Zigzag Turning of Bombyx mori Males during Pheromone-mediated Upwind Walking(Physology). *Zoological science.* **9**, 515–527 (1992).
13. Namiki, S. & Kanzaki, R. The neurobiological basis of orientation in insects: insights from the silkmoth mating dance. *Current Opinion in Insect Science* **15**, 16–26 (2016).
14. Wystrach, A., Lagogiannis, K. & Webb, B. Continuous lateral oscillations as a core mechanism for taxis in Drosophila larvae. *eLife* **5**, e15504 (2016).
15. Kuenen, L. P. S. & Baker, T. C. A non-anemotactic mechanism used in pheromone source location by flying moths. *Physiol Entomol* **8**, 277–289 (1983).
16. Olberg, R. M. Pheromone-triggered flip-flopping interneurons in the ventral nerve cord of the silkworm moth,Bombyx mori. *J. Comp. Physiol.* **152**, 297–307 (1983).
17. Namiki, S., Iwabuchi, S., Pansopha Kono, P. & Kanzaki, R. Information flow through neural circuits for pheromone orientation. *Nat Commun* **5**, 5919 (2014).
18. Hangartner, W. Spezifit/it und Inaktivierung des Spurphcromons yon Lasius fuliginosus Latr. und Orientierung der Arbeiterinnen im Duftfeld. *Springer* **57**, 34 (1967).
19. Izquierdo, E. J. & Lockery, S. R. Evolution and Analysis of Minimal Neural Circuits for Klinotaxis in Caenorhabditis elegans. *Journal of Neuroscience* **30**, 12908–12917 (2010).
20. Adden, A., Stewart, T. C., Webb, B. & Heinze, S. *A neural model for insect steering applied to olfaction and path integration*. http://biorxiv.org/lookup/doi/10.1101/2020.08.25.266247 (2020) doi:10.1101/2020.08.25.266247.
21. Kodzhabashev, A. & Mangan, M. Route Following Without Scanning. in *Biomimetic and Biohybrid Systems* (eds. Wilson, S. P., Verschure, P. F. M. J., Mura, A. & Prescott, T. J.) vol. 9222 199–210 (Springer International Publishing, 2015).
22. Le Möel, F. & Wystrach, A. Opponent processes in visual memories: A model of attraction and repulsion in navigating insects' mushroom bodies. *PLoS Comput Biol* **16**, e1007631 (2020).
23. Murray, T. *et al.* The role of attractive and repellent scene memories in ant homing (*Myrmecia croslandi*). *J Exp Biol* **223**, jeb210021 (2020).

24. Graham, P. & Collett, T. S. View-based navigation in insects: how wood ants (*Formica rufa* L.) look at and are guided by extended landmarks. *Journal of Experimental Biology* **205**, 2499–2509 (2002).
25. Lent, D. D., Graham, P. & Collett, T. S. Phase-Dependent Visual Control of the Zigzag Paths of Navigating Wood Ants. *Current Biology* **23**, 2393–2399 (2013).
26. Lent, D. D., Graham, P. & Collett, T. S. Image-matching during ant navigation occurs through saccade-like body turns controlled by learned visual features. *Proceedings of the National Academy of Sciences* **107**, 16348–16353 (2010).
27. Jayatilaka, P., Murray, T., Narendra, A. & Zeil, J. The choreography of learning walks in the Australian jack jumper ant *Myrmecia croslandi*. *J Exp Biol* **221**, jeb185306 (2018).
28. Zeil, J. & Fleischmann, P. N. The learning walks of ants (Hymenoptera: Formicidae). (2019) doi:10.25849/MYRMECOL.NEWS_029:093.
29. Stürzl, W., Zeil, J., Boeddeker, N. & Hemmi, J. M. How Wasps Acquire and Use Views for Homing. *Current Biology* **26**, 470–482 (2016).
30. Voss, R. & Zeil, J. Active vision in insects: an analysis of object-directed zig-zag flights in wasps (Odynerus spinipes ?, Eumenidae). *Journal of Comparative Physiology A: Sensory, Neural, and Behavioral Physiology* **182**, 377–387 (1998).
31. Philippides, A., de Ibarra, N. H., Riabinina, O. & Collett, T. S. Bumblebee calligraphy: the design and control of flight motifs in the learning and return flights of Bombus terrestris. *Journal of Experimental Biology* **216**, 1093–1104 (2013).
32. Jayatilaka, P., Raderschall, C. A., Narendra, A. & Zeil, J. Individual foraging patterns of the jack jumper ant Myrmecia croslandi (Hymenoptera: Formicidae). *Myrmecological News* **19**, 75–83 (2013).
33. Narendra, A., Gourmaud, S. & Zeil, J. Mapping the navigational knowledge of individually foraging ants, *Myrmecia croslandi*. *Proc. R. Soc. B* **280**, 20130683 (2013).

34. Zeil, J., Narendra, A. & Stürzl, W. Looking and homing: how displaced ants decide where to go. *Phil. Trans. R. Soc. B* **369**, 20130034 (2014).
35. Card, A., McDermott, C. & Narendra, A. Multiple orientation cues in an Australian trunk-trail-forming ant, Iridomyrmex purpureus. *Aust. J. Zool.* **64**, 227 (2016).
36. Collett, M. & Collett, T. S. Path Integration: Combining Optic Flow with Compass Orientation. *Current Biology* **27**, R1113–R1116 (2017).
37. Heinze, S., Narendra, A. & Cheung, A. Principles of Insect Path Integration. *Current Biology* **28**, R1043–R1058 (2018).
38. Muller, M. & Wehner, R. Path integration in desert ants, Cataglyphis fortis. *Proceedings of the National Academy of Sciences* **85**, 5287–5290 (1988).
39. Collett, T. S. & Cartwright, B. A. Eidetic images in insects: their role in navigation. at https://doi.org/10.1016/0166-2236(83)90048-6. (1983).
40. Zeil, J. Visual homing: an insect perspective. *Current Opinion in Neurobiology* **22**, 285–293 (2012).
41. Dahmen, H., Wahl, V. L., Pfeffer, S. E., Mallot, H. A. & Wittlinger, M. Naturalistic path integration of *Cataglyphis* desert ants on an air-cushioned lightweight spherical treadmill. *J Exp Biol* **220**, 634–644 (2017).
42. Lonnendonker, U. DYNAMIC PROPERTIES OF ORIENTATION TO A VISUALLY FIXATED TARGET BY WALKING COLORADO BEETLES. *Journal of Experimental Biology* **158**, 16 (1991).
43. Zollikofer, C. P. E. STEPPING PATTERNS IN ANTS. *Journal of Experimental Biology* **192**, 107–118 (1994).
44. Namiki, S. & Kanzaki, R. Comparative Neuroanatomy of the Lateral Accessory Lobe in the Insect Brain. *Front. Physiol.* **7**, (2016).
45. Steinbeck, F., Adden, A. & Graham, P. Connecting brain to behaviour: a role for general purpose steering circuits in insect orientation? *J Exp Biol* **223**, jeb212332 (2020).

46. Berni, J. Genetic Dissection of a Regionally Differentiated Network for Exploratory Behavior in Drosophila Larvae. *Current Biology* **25**, 1319–1326 (2015).
47. Berni, J., pulver, S. R., Griffith, L. C. & Bate, M. Autonomous Circuitry for Substrate Exploration in Freely Moving Drosophila Larvae. *Current Biology* **22**, 10 (2012).
48. Kanzaki, R. Neural Basis of Odor-source Searching Behavior in Insect Brain Systems Evaluated with a Mobile Robot. *Chemical Senses* **30**, i285–i286 (2005).
49. Baddeley, B., Graham, P., Husbands, P. & Philippides, A. A Model of Ant Route Navigation Driven by Scene Familiarity. *PLoS Comput Biol* **8**, e1002336 (2012).
50. Kamhi, J. F., Barron, A. B. & Narendra, A. Vertical Lobes of the Mushroom Bodies Are Essential for View-Based Navigation in Australian Myrmecia Ants. *Current Biology* **30**, 3432-3437.e3 (2020).
51. Wystrach, A., Mangan, M., Philippides, A. & Graham, P. Snapshots in ants? New interpretations of paradigmatic experiments. *Journal of Experimental Biology* **216**, 1766–1770 (2013).
52. Brembs, B. The brain as a dynamically active organ. *Biochemical and Biophysical Research Communications* **564**, 55–69 (2021).
53. Schroeder, C. E., Wilson, D. A., Radman, T., Scharfman, H. & Lakatos, P. Dynamics of Active Sensing and perceptual selection. *Current Opinion in Neurobiology* **20**, 172–176 (2010).
54. Yuste, R., MacLean, J. N., Smith, J. & Lansner, A. The cortex as a central pattern generator. *Nat Rev Neurosci* **6**, 477–483 (2005).
55. Hindmarsh Sten, T., Li, R., Otopalik, A. & Ruta, V. Sexual arousal gates visual processing during Drosophila courtship. *Nature* **595**, 549–553 (2021).
56. Kanzaki, R. & Mishima, T. Pheromone-Triggered 'Fiipflopping' Neural Signals Correlate with Activities of Neck Motor Neurons of a Male Moth, Bombyx mori. *Zoological Science* **13**, 79–87 (1996).

57. Egelhaaf, M., Boeddeker, N., Kern, R., Kurtz, R. & Lindemann, J. P. Spatial vision in insects is facilitated by shaping the dynamics of visual input through behavioral action. *Front. Neural Circuits* **6**, (2012).
58. Marder, E. & Calabrese, R. L. Principles of rhythmic motor pattern generation. *Physiological Reviews* **76**, 687–717 (1996).
59. McAuley, J. H., Rothwell, J. C. & Marsden, C. D. Human anticipatory eye movements may reflect rhythmic central nervous activity. *Neuroscience* **94**, 339–350 (1999).
60. Keijzer, F., van Duijn, M. & Lyon, P. What nervous systems do: early evolution, input–output, and the skin brain thesis. *Adaptive Behavior* **21**, 67–85 (2013).
61. Buehlmann, C. *et al.* Mushroom Bodies Are Required for Learned Visual Navigation, but Not for Innate Visual Behavior, in Ants. *Current Biology* **30**, 3438-3443.e2 (2020).
62. Webb, B. & Wystrach, A. Neural mechanisms of insect navigation. *Current Opinion in Insect Science* **15**, 27–39 (2016).
63. Pansopha, P., Ando, N. & Kanzaki, R. Dynamic use of optic flow during pheromone tracking by the male silkmoth, Bombyx mori. *Journal of Experimental Biology* **217**, 1811–1820 (2014).
64. Busch, C., Borst, A. & Mauss, A. S. Bi-directional Control of Walking Behavior by Horizontal Optic Flow Sensors. *Current Biology* **28**, 4037-4045.e5 (2018).
65. Wystrach, A. Movements, embodiment and the emergence of decisions. Insights from insect navigation. *Biochemical and Biophysical Research Communications* S0006291X21007348 (2021) doi:10.1016/j.bbrc.2021.04.114.
66. Wystrach, A., Philippides, A., Aurejac, A., Cheng, K. & Graham, P. Visual scanning behaviours and their role in the navigation of the Australian desert ant Melophorus bagoti. *J Comp Physiol A* **200**, 615–626 (2014).
67. Schwarz, S., Clement, L., Gkanias, E. & Wystrach, A. *How do backward walking ants (* Cataglyphis velox *) cope with navigational uncertainty?*

http://biorxiv.org/lookup/doi/10.1101/2019.12.16.877704 (2019) doi:10.1101/2019.12.16.877704.

68. Wystrach, A., Le Moël, F., Clement, L. & Schwarz, S. *A lateralised design for the interaction of visual memories and heading representations in navigating ants*. http://biorxiv.org/lookup/doi/10.1101/2020.08.13.249193 (2020) doi:10.1101/2020.08.13.249193.
69. Heinze, S., Florman, J., Asokaraj, S., el Jundi, B. & Reppert, S. M. Anatomical basis of sun compass navigation II: The neuronal composition of the central complex of the monarch butterfly. *J. Comp. Neurol.* **521**, 267–298 (2013).
70. Sayre, M. E., Templin, R., Chavez, J., Kempenaers, J. & Heinze, S. A projectome of the bumblebee central complex. *eLife* **10**, e68911 (2021).
71. Hulse, B. K. *et al.* A connectome of the Drosophila central complex reveals network motifs suitable for flexible navigation and context-- dependent action selection. 180.
72. Stone, T. *et al.* An Anatomically Constrained Model for Path Integration in the Bee Brain. *Current Biology* **27**, 3069-3085.e11 (2017).
73. Le Moël, F., Stone, T., Lihoreau, M., Wystrach, A. & Webb, B. The Central Complex as a Potential Substrate for Vector Based Navigation. *Front. Psychol.* **10**, 690 (2019).

STAR methods

RESOURCE AVAILABILITY :

Lead contact

Further information and requests for resources and reagents should be directed to and will be fulfilled by the lead contact, Leo Clement (clement.leo@univ-tlse3.fr).

Materials availability

As experiments took place in the natural environment this study did not generate new unique reagents.

Data and code availability

Any data or code information required to generate this results paper is available from the lead contact upon request.

- All data reported in this paper will be shared by the lead contact upon request
- All original code has been deposited at: https://github.com/awystrac/Neural_oscillator and is publicly available as of the date of publication.
- Any additional information required to reanalyze the data reported in this paper is available from the lead contact upon request

EXPERIMENTAL MODEL AND SUBJECT DETAILS

Study Animal & Experimental site

All experiments took place within an open grassy woodland at the National Australian University, Canberra from Feb. to Mar. 2019. We had the opportunity to work with two Australian endemic ant species: *Myrmecia croslandi* and *Iridomyrmex purpureus*. *Myrmecia croslandi* workers are known to forage solitarily, with each individual either hunting on the ground in the vicinity of the nest or navigating routinely back and forth toward the same favorite foraging tree throughout her life span[66]. These ants rely mainly on learnt terrestrial visual cues to navigate but are also able to resort to PI when the visual environment does not provide guidance[27,32,39,66]. Eight nests of *M. croslandi*, that foraged on two distinct trees between 6.0 and 30.0 m away from the colony, were used in this study. *Iridomyrmex purpureus* ants form large colonies and forage along pheromone trails that lead to food patches. Despite employing pheromone trails for recruitment, this species also uses both learnt visual information and path integration for navigation[31]. We also performed navigational experiments with two *I. purpureus* nests to ensure that this species relies indeed on both learnt visual terrestrial cues and path integration, which they did surprisingly well (see Figure S1). For the main experiment, a feeder was placed 7.0 m away from the nest and foragers were free to familiarize themselves with the route for 72 h before being tested.

METHOD DETAILS

Trackball system and data extraction

During tests, ants were mounted on a trackball device[38]. This device consists of a polystyrene ball held in levitation in an aluminum cup by an air flow. The trackball has two sensors placed at 90° to the azimuth of the sphere, which record the movements of this sphere and translate them into X and Y data retracing the path of the ant. The X and Y acquisition of the trackball rotations happened at a 30 Hz frequency (i.e., 30 data points per second), enabling us to reconstruct the ant's movements with high precision. Additionally, a camera (640×480 pixels) recording from above provided details of the ant's body orientation, also at 30 Hz. We also analyzed *M. croslandi* learning walks recorded directly on the natural ground. Head directions were obtained via video recordings at 25 Hz (provided by Jochen Zeil).

In this study, we used two different trackball configurations to record the ants' motor responses: further referred to as 'Free ant' and 'Fixed ant' experiments, respectively.

Free ant experiments: two small wheels prevented the polystyrene ball from rotating in the horizontal plane, however, all other degrees of freedom of the ball rotation were accessible (Figure S2 A; 'closed-loop'[38]). Ants were attached on top of the ball by putting magnetic paint on their thorax and a micro-magnet fixed at the bottom end of a single dental thread that was in turn attached to a 0. 5 mm pin. Crucially, the pin was placed within a glass capillary. This procedure enabled the ants to execute physical rotations on the ball (the ball is not rotating horizontally) but prevented any translational movement. Ants could thus execute body rotations and control the direction in which they faced but any attempt to go forward or backward resulted in ball rotations. We used the recorded videos to manually track the ants' body orientation through time using the free software Kinovea (v-0.9.1).

Fixed ant experiment: the two small wheels were no longer in place. Hence, the ball could now turn in any direction, including the horizontal plane (Figure S2B; 'open-loop'[38]). Ants were tethered directly to a needle with a micro magnet (glued at the end of the needle)

and magnetic paint on their thorax. The top end of the needle was glued to a small piece of paper sheet (0.5×2.5 cm). Consequently, the fixed ant could no longer rotate, and the experimenter could choose in which direction she was facing. Any attempt to move, including turning, by the ants resulted in ball rotations. This trackball configuration was only conducted with the more robust *M. croslandi*.

Free ant experiments: protocol

At the start of each test, the ant was mounted on the trackball device but surrounded by an opaque cylinder (30×30 cm) that prevented the ant from seeing any cues from the visual scenery around her. Once the ant was in place on the device, the whole apparatus was moved to the desired test location in the field. Afterward, the surrounding cylinder was removed, revealing the visual scenery to the ant and data recording began. To ensure a high level of homing motivation, only individuals who had previously received a 40% sucrose solution (for *M. croslandi*) or a food item (for *I. purpureus*) were tested. The recording period was 3.5 min for the robust *M. croslandi* and 1.5 min for the flimsier *I. purpureus*.

To test the impact of terrestrial visual cues on the oscillation behavior, ants were tested under three distinct conditions.

Familiar (F): ants were tested along their habitual route, which therefore presents a familiar visual view.

Unfamiliar (U): ants were tested at least 50 m away from the habitual route, which therefore presents an unfamiliar panorama.

Dark (D): ants were tested in total darkness, within an opaque cylinder (30×30 cm) covered with a red Plexiglas plate that transmitted only the low red wavelengths, which ants cannot perceive[67,68].

To test the impact of PI on oscillation behavior, ants were tested as either full- or zero vector ants. Full vector (FV): ants were caught at the start of their inbound trip to the nest (i.e., at the foraging tree for *M. croslandi* and at the feeder for *I. purpureus*). FV ants have an informative homing PI vector, which points in the food-to-nest compass direction. Consequently, FV ants can rely on both PI vector and the learnt visual scenery while being tested. Zero vector (ZV): homing ants were captured just before entering the nest, that is, at the end of their inbound trip. Hence, their PI homing vector is reduced to zero and thus no longer directionally informative. Consequently, ZV ants can only rely on the learnt visual scenery while being tested. For each of the three visual conditions FV and ZV ants were tested, resulting in a total of six conditions.

For *I. purpureus*, at least 16 ants were tested in each of the six conditions (F: FV&ZV =16; U: FV&ZV =17; D: FV=16 & ZV=17). Since *I. purpureus* forms very populous colonies with an abundance of foragers, all individuals were tested only once, in one of the six conditions. The data obtained are therefore statistically independent. On the contrary, *M. croslandi* forms sparsely populated colonies and individuals usually make only one foraging trip per day[66]. Thus, it is time-consuming and challenging to capture, mark and follow individuals throughout foraging trips. Individuals were therefore captured (either at the foraging tree (FV) or before reaching their nest (ZV)) and tested successively in a pseudo-random order in all three visual panoramas: Familiar (F), Unfamiliar (U) and in the Dark (D). Both the sequence in which the visual conditions were experienced and the individuality were included in the statistical models as it is likely that the state of the PI vector will be modified across successive tests. Overall, 32 *M. croslandi* ants were tested with some individuals

tested as ZV or FV ants on two different days. At least 16 *M. croslandi* ants were tested in each of the six conditions (F: FV&ZV =17; U: FV&ZV =17; D: FV=17 & ZV =16). Overall, 101 recordings were obtained.

In the 'free ant' experiments, the ant's body axis can turn without the ball movement. We used the recorded videos to manually track the ants' body orientation through time using the free software Kinovea. We removed the first 3s of recording of each ant as the removal of the opaque ring may have disrupted the behavior. Overall, the analyzed recording length was 100s (except for two ants: 84 and 99s) for *M. croslandi* individuals and 50s (except for two ants: 49s) for *I. purpureus* ants. For details of the Fourier analysis (see below); nine paths of *I. purpureus* were discarded (F FV=1, U FV = 1, U ZV =2, D FV =2, D ZV = 3) as the ants displayed too many pauses.

Fixed ant experiments: protocol

To test if oscillations are due to an intrinsic oscillator or caused by the fact that ants try to keep a bearing toward an external stimulus, we conducted an additional experiment on *M. croslandi* ants. We recorded foragers without an informative integration vector (ZV) in the same unfamiliar environment (U) as before. Ants were tested in eight different fixed orientations, covering the 360° azimuth by bins of 45°; and with one direction corresponding to the food-to-nest compass direction. Each ant was tested in all eight orientations in a pseudo-random sequence. To change the ant's orientation, the experimenter would first place the opaque cylinder (30×30 cm) around the trackball system to prevent the ant from perceiving the visual panorama, then rotate the whole set-up (trackball and mounted ant) and finally remove the opaque cylinder to re-start data collection. Ants were recorded for at least 15s up to 20s in each orientation. Eleven ants were tested in all eight orientations. Since the

ants were fixed, trackball rotations along the horizontal axis provided a direct measure of the angular velocity of the attempted turn generated by the ant. Angular velocity time series were then extracted from the trackball data. At the end, the available length of the recordings for the analysis had 512 frames (~17s) except for 5 individuals (294,394,456,474,494 frames). It should be noted here that prior to the Fourier analysis (see below) we added a series of 0s (zero padding) at the end of the time series until it had a length of 3000 data points to match the same recording length obtained in the free ant experiment). This permits to increases the precision in the frequency range obtained from the Fourier analysis.

QUANTIFICATION AND STATISTICAL ANALYSIS

All statistical analyses have been run using the free software R (v 3.6.2. R Core Development Team). For all statistical tests, the p-values were compared to the critical alpha risk at 0.05, with the appropriate correction if needed. Statistical parameters mean and the associated standard error is given within the text and/or on figures: N represents the number of individuals.

Fourier analysis

To reveal the occurrence of regular lateral oscillations, we choose to focus on the angular velocity value (Figure S2C), which constitutes a direct reading from the left/right motor control. This time series was processed through three successive steps to obtain its ‘spectral density’, according to the Wiener-Khinchin theorem. First, the signal was parsimoniously smoothed with a moving median running of a length of five frames (0.17s) to reduce the influence of the recording noise (Figure S2D, dashed blue line). Then, the recorded time series was passed through an autocorrelation function (Figure S2D). Finally, a Fourier transform was performed on these autocorrelation coefficients, providing the power spectral

density (Figure S2E). With this approach, the magnitudes obtained are independent from angular drift and amplitudes of the oscillations and thus can be directly compared across individuals. A high magnitude indicates a strong oscillation for a given frequency. For each individual, the dominant frequency (i.e., presenting the highest peak magnitude) and its magnitude were extracted (Figure S2E, dashed blue lines). To check whether these magnitudes indicate a significant regular oscillation, we compared them to the average spectral density magnitude resulting from 200 Gaussian white noise signals of the same length (within each species and experiment). Gaussian white noise signals were obtained by drawing a sequence of random values drawn from a normal law. These simulated signals were then processed through the exact same operations as the ants' angular velocity recording: namely smoothing, autocorrelation, Fourier transformation and extraction of the highest peak magnitude. The mean of the 200 highest magnitudes obtained was then compared to the real ants' equivalent magnitudes with a Wilcoxon one-tail test. As each experimental group has been compared with this mean magnitude of the simulated angular velocity signal, the p-value is subsequently adjusted using the Bonferroni correction.

Average oscillatory cycle

To extract the average dynamics of an oscillation cycle, the mean cycles at the individual and population levels were reconstructed as follows. First, we smoothed the angular velocity time series of each individual by running twice a median with a window length of 31 frames for *M. croslandi* (for both free and fixed experiments), 25 frames for data during learning walks on the natural ground and seven frames for *I. purpureus*. This window length is much smaller than one oscillatory cycle and thus smoothens the data without altering the cycle general dynamics (Figure S5 A). Second, we indexed moments when the time series crosses 0 (from

– to +) as t_0; and extracted a window of ±90 frames around the t_0 indices (±60 frames for *I. purpureus*; Figure S5 A). We then reconstructed a mean cycle for each individual by averaging the individual's extracted windows, aligned at t_0 (Figure S5 B). The individuals' average forward speed dynamics during one cycle was obtained in the same way by using the same indices t_0 obtained from the angular velocity data (Figure S5 C). For each ant, the mean angular velocity peak and amplitude of forward velocity cycles were extracted for analysis. Finally, we reconstructed the average cycle at the level of the population by averaging the mean cycle of all individuals. Note that to do so, each individual's mean cycle was first normalized to show similar amplitudes (mean_cycle_normalised = mean_cycle/mean|mean_cycle_values|). The goal was here to observe the cycle dynamics through time and not to estimate the inter-individual variation in amplitude, which was analyzed previously using the individual's mean cycle amplitude. Note that the criterion used to align the time series (the change from a left to a right turn) necessarily creates an artefact in the averaged angular velocity obtained. Namely, an average change from left turn to right turn at t_0. However, several factors indicate the relevance of such pooling at the population level: (1) the period of the average cycle corresponds to the mean frequency obtained from the Fourier transform. (2) we can observe a significant reversal of the angular velocity before and after the mean oscillation cycle. (3) the associated forward velocities co-vary in a significant way, indicating the existence of conserved dynamics.

Analysis of the ants' direction of movement

We reconstructed the ant paths of time that derived from the trackball recording for a fixed period to determine the mean direction of movement (mu) as well as the mean circular vector length (r, a measure of dispersion) of each individual. The mean directions (mu) were

analyzed using a Rayleigh test (from R package: Circular) that also includes a theoretical direction (analogous to the V-test). To test whether the angular data are distributed uniformly as a null hypothesis or if they are oriented toward the theoretical direction of the nest as indicated by the state of the PI or the familiar panorama, the average vectors lengths (r) were analyzed via a Wilcoxon-Mann-Whitney test with a Bonferroni correction for multiple testing.

Analysis of optimization

To investigate the benefit of variation of forward and angular velocities signal on the overall ground distance covered we reconstructed for each individual a fictive path where forward speed was maintained constant (we took the average forward speed, so that the total distance walked remain the same as in the original path). To estimate the overall ground distance covered for a given path, we computed a 'global trajectory' by smoothing the path with a sliding window, until effectively removing the oscillations component (Figure 4B grey paths). To estimate the actual benefit of variation of forward speed on the distance covered, we compared the length of the 'global trajectories' between the fictive path (with constant forward speed) and original path (Fig 4C). A ratio >1 mean that the original path covered more ground distance, and vice versa. Ratios were compared with Wilcoxon one-tail test to the threshold one.

To test for an effect of the familiarity and vector on the distance covered we calculated an 'Effectiveness ratio' for each individual as the ratio between the length of the 'global trajectory' / 'actual distance walked' on the original paths with oscillations (Figure 4D). To

enable a fair comparison across individuals, we computed the “effectiveness ratio” on a 100s portion of paths, using an additive mixed model.

Statistical models

For the free ant experiment, two types of models were tested: the first considering the interaction between visual panorama and vector modalities, the second with simple additive effect. It should be noted here that in case of deviation of the residuals of these models from normality and or homoscedasticity, the response variables have been transformed. Only the model presenting the lowest Akaike information criterion was retained and subsequently analyzed via an analysis of variance (Anova), followed by a post-hoc analysis of Tukey's rank comparison. Finally, for *M. croslandi* whose individuals were tested across several conditions, the models are mixed models that controlled the sequence and the individuality effect as random variable. For some models, we removed the sequence effect because of a singularity problem of this factor (i.e., the information given by this variable is already contained in other variables). For fixed ant experiments (which were tested only as ZV ants in an unfamiliar environment), the model analyzed the effect of the condition of the subsequent rotations.

COMPUTATIONAL MODEL

The computational model presented in Figure6 has been built and run using Matlab® R2016b. The code is open access and available at :

https://github.com/awystrac/Neural_oscillator

It is a step based model (‘For loop’). Two neurons (Left and Right neurons) reciprocally inhibit each other, while trying to maintain a baseline activity through self-excitation and internal feedback.

Variable	Description
L	Left neuron activity
R	Right neuron activity
LNF	Left neuron internal feedback
RNF	Right neuron internal feedback

Parameters	Description
W	Reciprocal inhibition synaptic weight
Baseline	Firing rate of the oscillator neurons without any external modulation (default at 0.5)
Exhaust rate	Rate at which the negative internal feedback is modulated between each time step
Noise	Standard error of the normal distribution of the noise added to the activity of the neurons of the oscillator (default at 0.1)

Initialization

R_1= random (0to1)

L_1 = random (0to1)

$RNF_1 = 0$

$LNF_1 = 0$

At each time step

L and R neuron update their activity due to their self-excitation, internal feedback, inhibition from the other neuron, and noise.

$$L_{t+1} = L_t - LNF_t - (R_t \times W) + (random(-1\ to\ 1) \times noise)$$

$$R_{t+1} = R_t - RNF_t - (L_t \times W) + (random(-1\ to\ 1) \times noise)$$

Set a hard limit to the activity both neurons

$$LM_{t+1} = \begin{cases} L_{t+1} & if\ L_{t+1} > 0 \\ 0 & if\ L_{t+1} \leq 0 \end{cases} \qquad RM_{t+1} = \begin{cases} RM_{t+1} & if\ R_{t+1} > 0 \\ 0 & if\ R_{t+1} \leq 0 \end{cases}$$

Update the internal negative feedback for the left and right motor neurons. The internal feedback changes proportionally to the difference between its own activity and the neuron activity (relative to the baseline activity)

$$RNF_{t+1} = RNF_t + \text{Exhaust rate} \times (R_{t+1} - RNF_t - \text{Baseline})$$

$$LNF_{t+1} = LNF_t + \text{Exhaust rate} \times (L_{t+1} - LNF_t - \text{Baseline})$$

Computation of the angular and forward velocities

Angular_velocity = R - L

Foward_velocity = R + L

Supplemental information 1

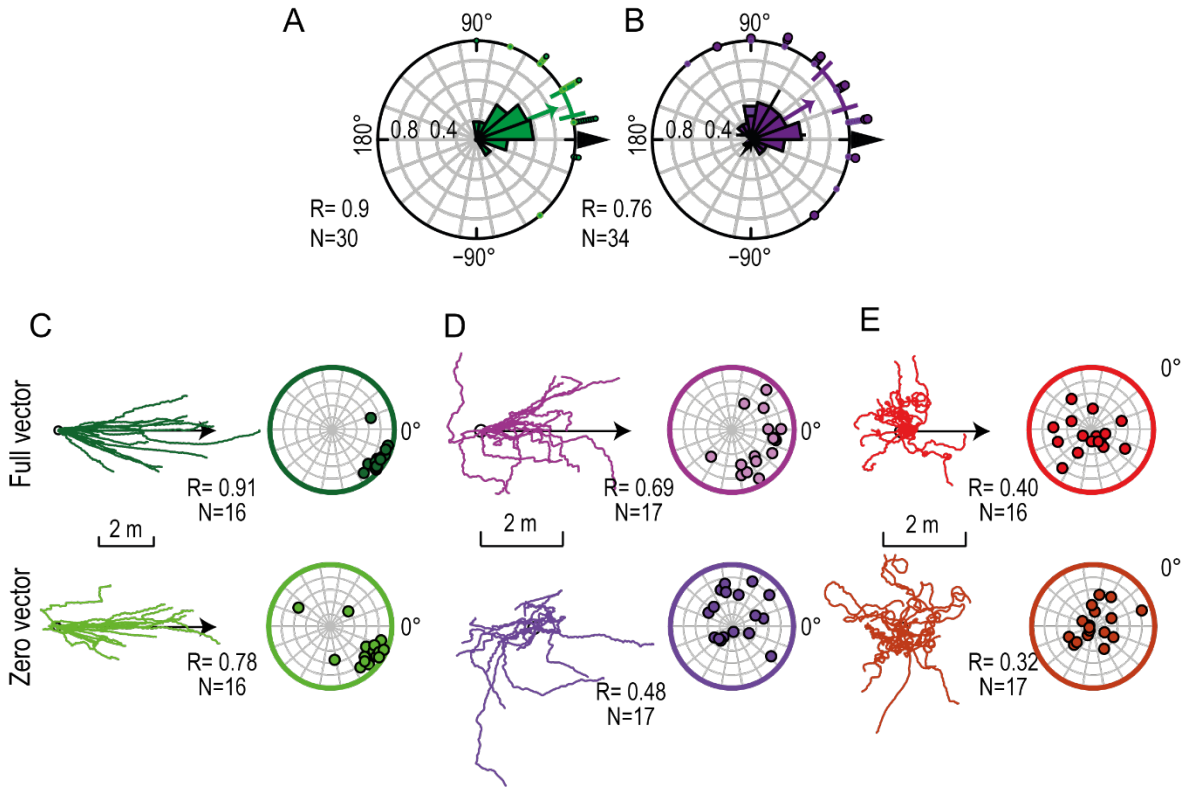

Figure S1: The meat ant *Iridomyrmex purpureus* uses both visual and celestial cues to navigate. (A-B) Ants were released at the center of a goniometer divided in 18 sectors (20° each) either in a familiar (green) or unfamiliar (purple) surroundings. The taken directions of the tested ants were recorded at two points. (A) Circular histogram depicting the directional decisions of tested zero-vector (ZV) ants (without informative integration vector) in presence of familiar surroundings. (B) Circular histogram depicting the directional decisions of tested full-vector (FV) ants (with informative integration vector) in unfamiliar surroundings. The arrow corresponds to the mean vector of the distribution. The 95% confidence interval of the mean is displayed as a coloured arc. Each dot corresponds to one corrected direction obtained from one individual. after several tested individuals, the goniometers were rotated (180°) to prevent the use of chemical trails. Dots with a black rim are data recorded before rotation of the goniometers and the dots without black rim after rotation.
(C-E) Path of ant reconstructed over 25 s from the trackball, in a familiar ((C) green) or an unfamiliar panorama ((D) purple) and in the dark ((E) red). For each condition, individuals were tested either as FV- or ZV vector ant. The first column of each condition shows the paths oriented to the theoretical direction of the nest (arrow). In the second column, each dot indicates the average circular vector calculated over the entire path of an individual, showing the mean direction and the average vector length (i.e., a point closer to the periphery indicates straighter paths). The R values indicate the length of the average resulting vector of the population. In all graphs, the direction (in familiar terrain) or theoretical direction (for FV in unfamiliar terrain) of the nest is set at 0°.
The results show that ants in presence of familiar panorama were oriented toward their nest irrespectively of the PI state (FV or ZV) (Rayleigh test: on goniometers (A): $p<0.001$; path displayed on the trackball (B): ps = FV & ZV < 0.001). Secondly, when tested in unfamiliar surroundings, FV ants followed their PI vector (Rayleigh test: on goniometers (B): $p<0.001$; path displayed on the trackball (D, first row): p = FV < 0.001). But ZV ants (Figure 1D

second row) showed random orientations (Rayleigh test p: ZV=0.672). Finally, ants displayed randomly orientated paths in all darkness conditions (Figure 1E; Rayleigh test p: FV=0.213, ZV=0.866). Overall, these results demonstrate that this species use learnt terrestrial cues as well as their PI to navigate when released on the goniometers or mounted on the trackball system. Therefore, in both experiment this species does not only rely on chemical trails but also on the visual panorama and the path integration during foraging.

Supplemental information 2

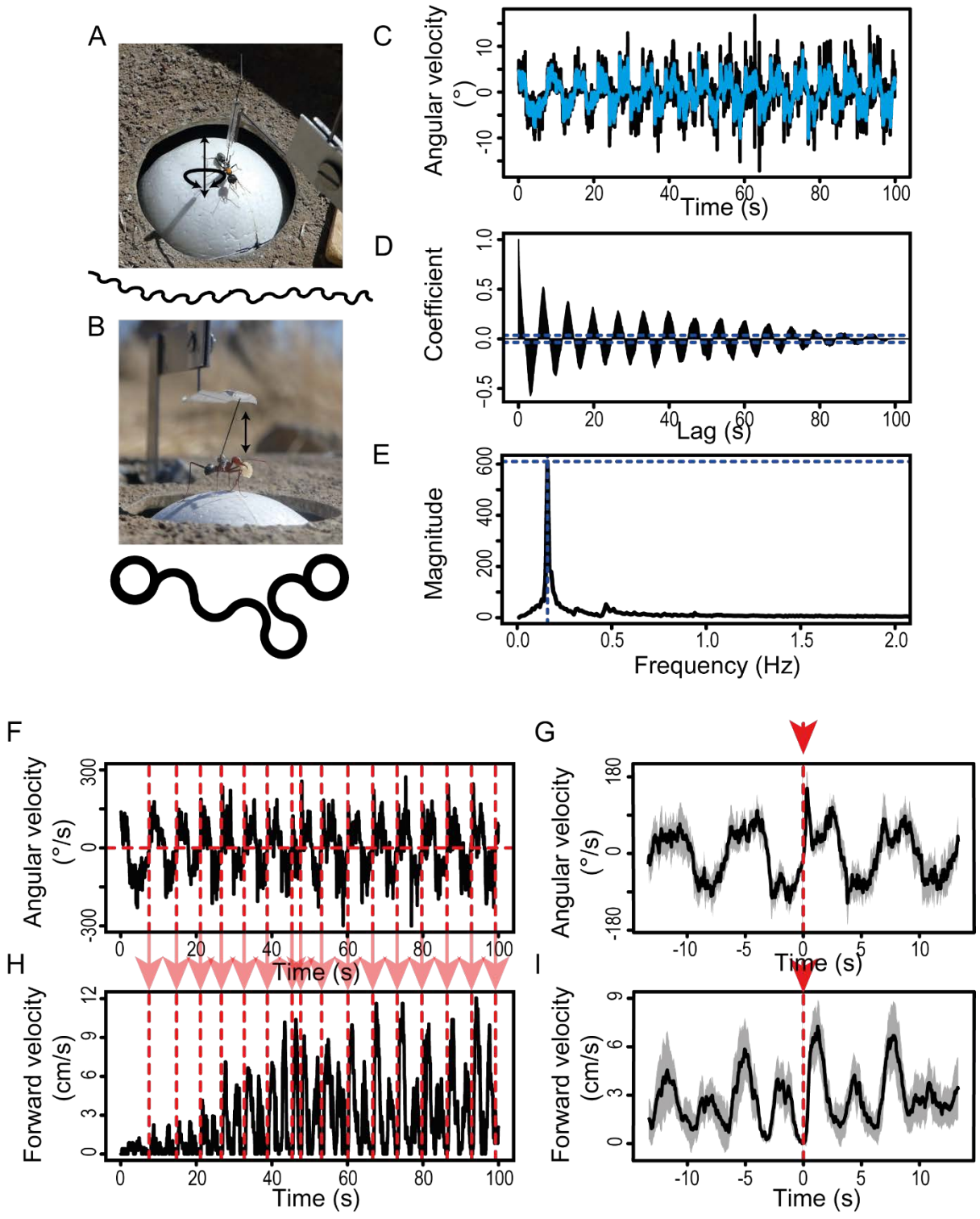

Figure S2: Trackball set-ups, recording and processing of the ants' trajectory. (A) Trackball set-up for 'free ant experiment' (top view). Two wheels prevent the sphere from rotating along the horizontal plane. Ants are free to rotate their body along the yaw axis to control in which direction they perceive the world. (B) Trackball set-up for 'fixed ant experiment' (side view). The two wheels have been removed, so the ball can turn in every direction. Ants are fixed in a way that prevent body rotations along the yaw axis, so they are

forced to keep their bearing in the imposed direction. For A and B an example path has been plotted below the picture. (C) Angular velocity signal over time (recorded at 30 readings/s) in an individual of the species *M. croslandi* (black) with smoothed signal superimposed (blue). (D) Autocorrelation carried out on the entire smoothed angular velocity signal. (E) Fourier transformation of the autocorrelation coefficients signal (shown in D) provides the 'spectral density'. This approach has the advantage to provide magnitudes that are directly comparable between individuals. For each individual, the frequency peak with the highest magnitude was extracted, indicating a strong oscillation of the angular velocity signal at that frequency (dashed blue lines). F-I Methodology to obtain an average oscillation cycle. (F) We used the angular velocity signal to flag moments when the signal crosses 0 and goes up to positive angles (vertical dashed red lines). (G) We extracted portions of the signal of ±3s (large enough to contain a full oscillation cycle) around each of the flags, aligned them at flag = t_0 and averaged them to obtain the individual's average cycle (±95% confidence interval in grey) of the angular velocity signal. (I) The individual's average cycle for the forward velocity signal was achieved using the angular velocity flags (vertical dashed red lines as in F) on the forward velocities (H).

Supplemental information 3

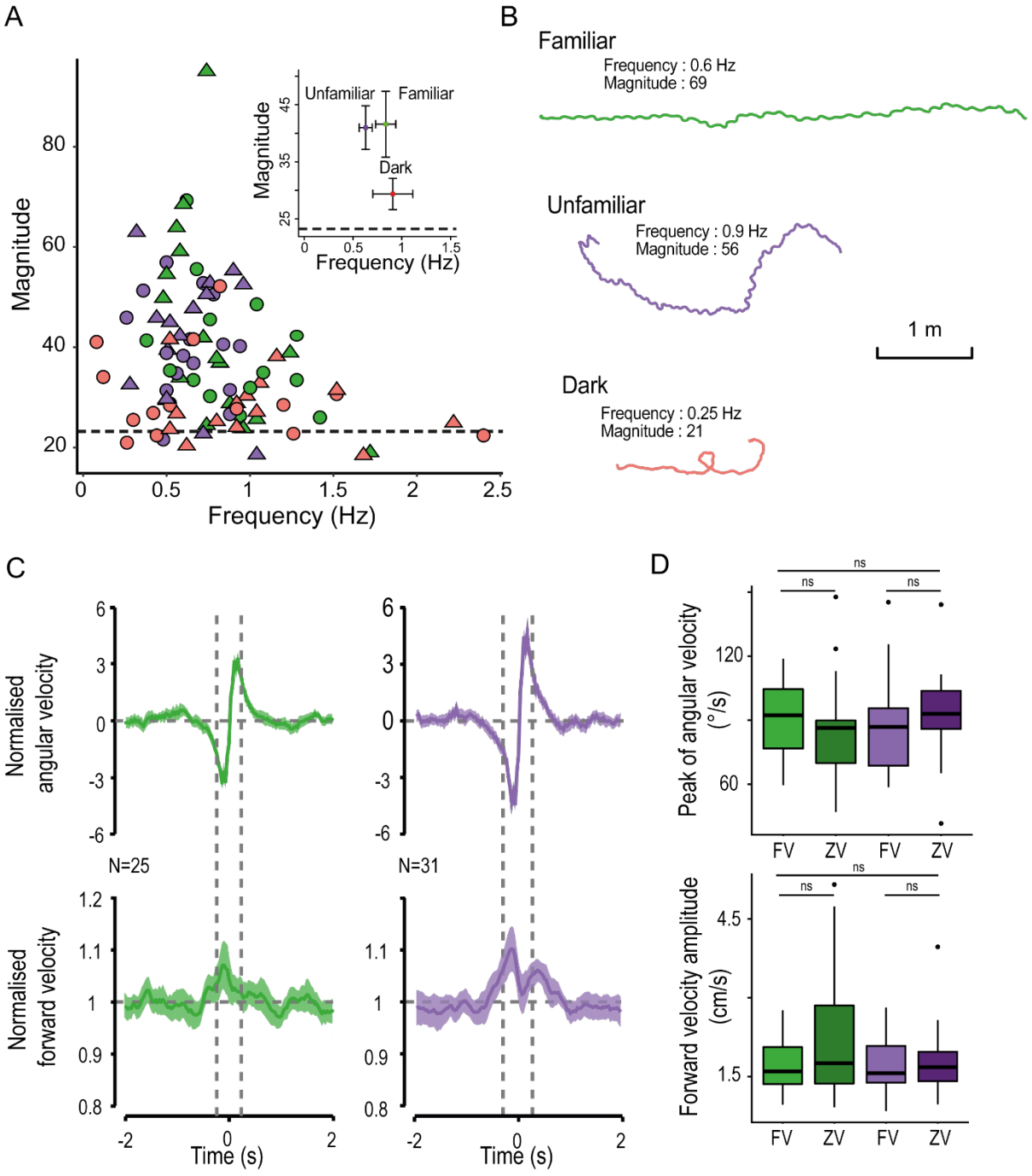

Figure S3: Oscillation characteristics across visual conditions.
Individuals were tested within a familiar panorama (green), an unfamiliar panorama (purple) or in the dark (red).
(A) shows the frequency and spectral density magnitude of the dominant oscillation (highest magnitude) (A) (for method see Star method and Figure S2 F-I). High frequencies indicate a fast-oscillatory rhythm and high magnitudes indicate a strong presence of this oscillation. Symbols indicate whether the state of the path integration vector was full (round) or set to zero (triangles). Inserts show the mean frequency against the mean magnitude of each visual condition with the associated 95% confidence interval around the mean. The dashed black

line represents the mean of the spectral density peak magnitudes resulting from 200 Gaussian white noise signals. Magnitudes were higher than those obtained with the spectral density of a Gaussian white noise ((A) dashed line; Wilcoxon one-tail test: ps≤0.01), showing that ants displayed lateral oscillations with a higher regularity than random. Analysis reveals that the regularity differ between visual panoramas with ants tested in familiar and unfamiliar terrain yield more regular oscillations than in the dark ((A) Anova: $F_{2,90}$=10.038, p < 0.001, F vs U = p>0.96, df=86, mean±se: $F_{(FV+ZV)}$ =41.59± 3; $U_{(FV+ZV)}$ =41±2 ; D vs U or F = p< 0.001, mean±se: $D_{(FV+ZV)}$=29.4±×1.45). However, independent of the PI state, ants showed a tendency to oscillate quicker in familiar than in unfamiliar terrain (ps ≥ 0.180, mean±se: mean±se: F(FV+ZV) =0.83±0.056 Hz; U(FV+ZV) =0.63±0.037).
(B) shows an example path for each condition across 83 s.
(C) Population-average cycle (see Star method and Figure S3) shows how angular and forward velocities co-vary. Angular velocities (top-row) and forward velocity (bottom row) co-vary in a way that is conserved across conditions: when on familiar route (green) or in unfamiliar terrain (purple). Population cycles have been reconstructed by merging full- (FV) and zero-vector (ZV) data and normalising the data amplitude within the individual's average cycle. Colour areas around the mean curves represent the 95% confidence interval, based on the inter-individual variation. Dashed lines represent the moment when the ants are facing their overall direction of travels. Angular velocities (top-row) and forward velocity (bottom row) co-varies in a way that seem conserved across experimental conditions and species (see Figure 3). (D) Boxplots show the actual distribution of the non-normalized mean peak of angular speed and forward velocity amplitude for the individuals' average cycle (FV on the left, ZV on the right). The mean peak of angular velocities and forward velocity amplitude underlying the oscillations are rather constant across navigational context ((D), (ps >0.05)). Therefore, there is no clear effect on the amplitude of oscillation display within the path (A, B).

Supplemental information 4

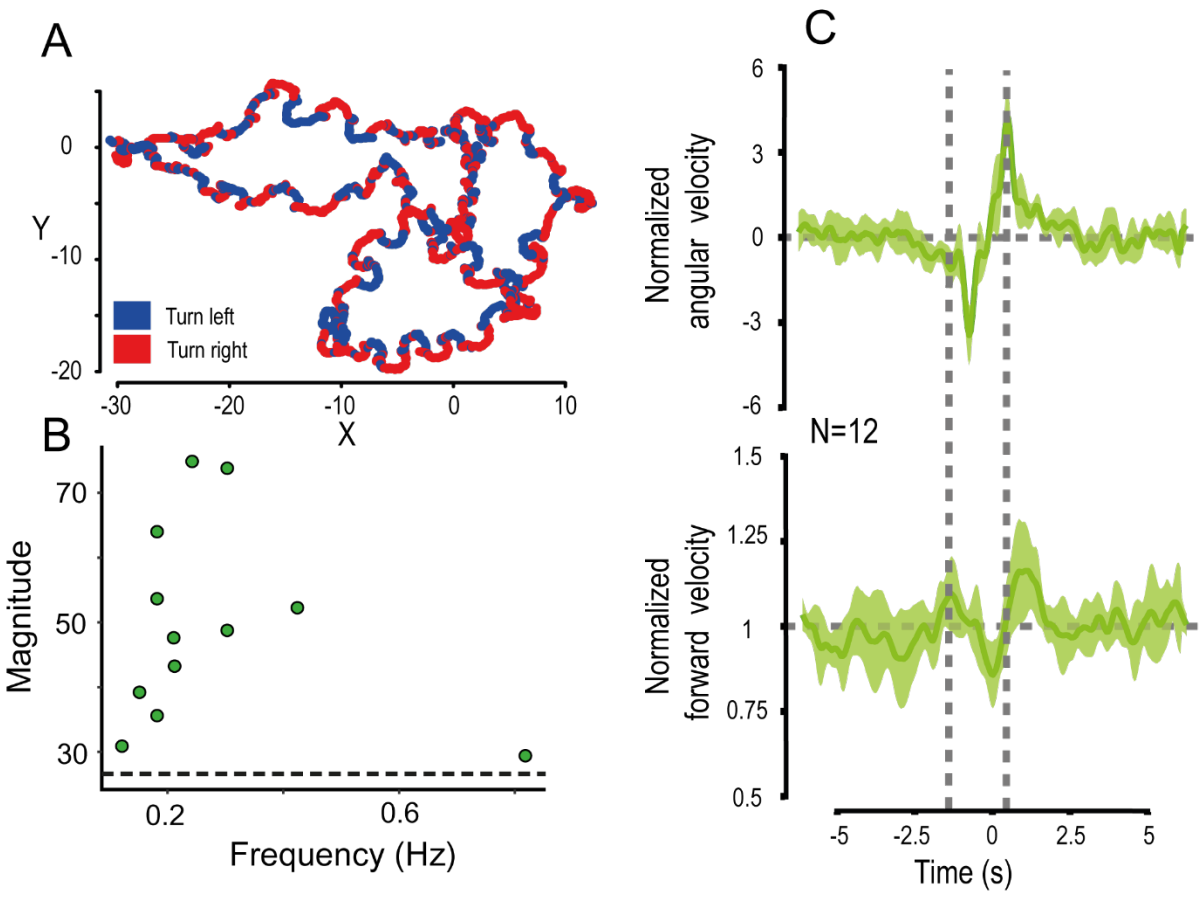

Figure S4. Ant learning walks show similar dynamics of oscillation. Ants path and head orientation were recorded (25 Hz) during their learning walks directly on the ground (courtesy of Jochen Zeil, see Jayatilaka et al, 2018). (A) Example path of an individual showing clear alternation between right (red) and left (blue) turn. (B) Frequency and spectral density magnitude of the dominant oscillation (highest magnitude) of angular velocities times series of 25s (for method see Star method and Figure S2 F-I). Magnitudes were higher than those obtained with the spectral density of a Gaussian white noise ((A) dashed line; Wilcoxon one-tail test: $p \leq 0.001$). (C) Angular velocity (top-row) and forward velocity (bottom row) co-vary in a similar way than when recorded on the track ball (see Figure 3). Population cycles have been normalised by the data amplitude within the individuals mean cycle (see Figure S*3* for example). Colour areas around the mean curves represent the 95% confidence interval, based on the inter-individual variation. The natural learning walks showed regular oscillations as well as the same dynamical relationship between angular and forward velocities than trackball data. Ants walking on the ground also tend to increase their forward velocity when they are aligned with their general direction of travel. Data provide by Jochen Zeil, see[27]

Supplemental information 5

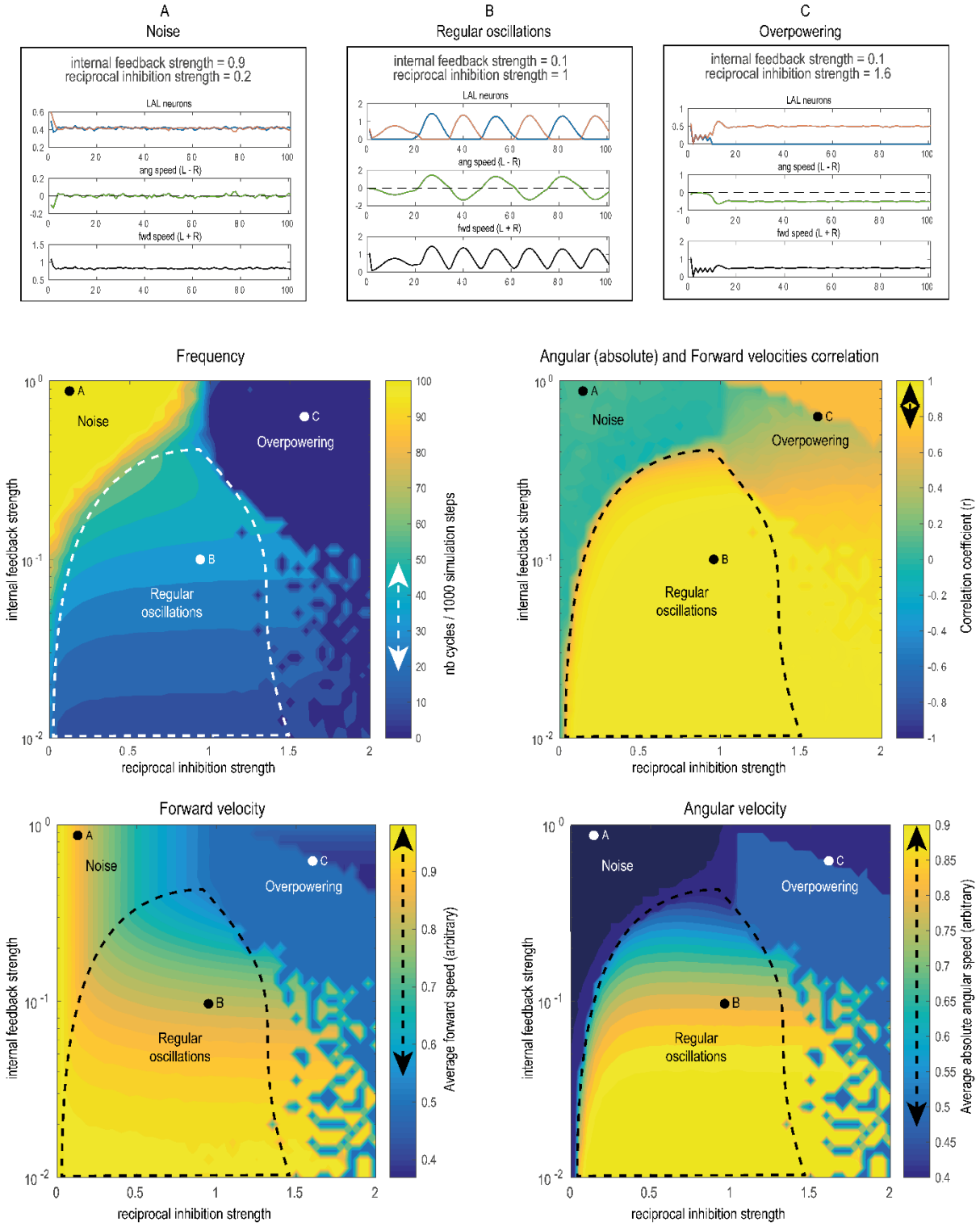

Figure S5. The covariation between angular and forward velocity is robust to parameter change. Exploration of our abstract LAL model's (Figure 5) sensitivity to change in the two free parameters (inhibition strength and internal feedback strength).

Regular oscillations between LAL neurons emerge in a wide space of parameters (functional range delineated by the dashed line, an example for a given parameter set (dot) is shown in (B)). While frequencies (right of middle row), forward and angular velocities (bottom row) can vary roughly across a factor 2 across the functional parameter range, the correlation between absolute angular and forward velocity is constrained around 1 (dashed arrows in the colour bars indicate the variation in the functional range). This positive covariation indicates that the agent slows down (low forward velocity) when reversing turning direction (low absolute angular velocity) and accelerates (high forward velocity) in between, that is when sweeping past its general direction of travel. Outside of this functional range, regular oscillations disappear for extreme parameter sets. For instance, if one neuron overpowers the other due to too strong reciprocal inhibitory strength (C, overpowering); or inversely, due to the absence of reciprocal inhibition (strength <0.01) or a too strong internal adaptation preventing the neurons to modulate their baseline activity, and thus resulting in noise (A).